

Fractal Dimension of Higher-Dimensional Chaotic Repellers

David Sweet and Edward Ott*

October 24, 2018

Institute for Plasma Research and Department of Physics
University of Maryland, College Park, Maryland 20742
dsweet@chaos.umd.edu
Ph: (301)405-1657 Fax: (301)405-1678

Abstract

Using examples we test formulae previously conjectured to give the fractal information dimension of chaotic repellers and their stable and unstable manifolds in “typical” dynamical systems in terms of the Lyapunov exponents and the characteristic escape time from the repeller. Our main example, a three-dimensional chaotic scattering billiard, yields a new structure for its invariant manifolds. This system also provides an example of a system which is not typical and illustrates how perturbation to the system restores typicality and the applicability of the dimension formulae.

PACS: 05.45.+b

1 Introduction

In addition to chaotic attractors, nonattracting chaotic sets (also called chaotic saddles or chaotic repellers) are also of great practical importance. In particular, such sets arise in the consideration of chaotic scattering, boundaries between basins of attraction, and chaotic transients. If a cloud of initial conditions is sprinkled in a bounded region including a nonattracting chaotic set, the orbits originating at these points eventually leave the vicinity of the set, and there is a characteristic escape time, τ , such that, at late time, the fraction of the cloud still in the region decays exponentially at the rate τ^{-1} .

The primary focus of this paper will be on studying the fractal dimension of nonattracting chaotic sets and their stable and unstable manifolds. Fractal

*Also Department of Electrical Engineering

dimension is of basic interest as a means of characterizing the geometric complexity of chaotic sets. In addition, a knowledge of the fractal dimension can, in some situations, provide quantitative information that is of potential practical use. For example, in the case of boundaries between different basins, the basin boundary is typically the stable manifold of a nonattracting chaotic set, and knowledge of the stable manifold's box-counting dimension (also called its capacity) quantifies the degree to which uncertainties in initial conditions result in errors in predicting the type of long-term motion that results (e.g., which attractor is approached; see Sec. 5 and Ref. [1]). Our focus is on obtaining the information dimension of a suitable "natural measure" μ lying on the chaotic set (see Sec. 2 for definitions of the natural measures for nonattracting chaotic sets and their stable and unstable manifolds). The information dimension is a member of a one parameter (q) class of dimension definitions given by

$$D_q = \lim_{\epsilon \rightarrow 0} \frac{1}{1-q} \frac{\ln \sum \mu_i^q}{\ln(1/\epsilon)}, \quad (1)$$

where q is a real index, ϵ is the grid spacing for a d -dimensional rectangular grid dividing the d -dimensional state space of the system, and μ_i is the natural measure of the i^{th} grid cube. The box-counting dimension is given by (1) with $q = 0$, and the information dimension is given by taking the limit $q \rightarrow 1$ in (1),

$$D_1 = \lim_{\epsilon \rightarrow 0} \frac{I(\epsilon)}{\ln(1/\epsilon)}, \quad I(\epsilon) = \sum_i \mu_i \ln(1/\mu_i). \quad (2)$$

In general, the information dimension is a lower bound on the box-counting dimension, $D_1 \leq D_0$. In practice, in cases where D_1 and D_0 have been determined for chaotic sets, it is often found that their values are very close.

We are specifically concerned with investigating formulae conjectured in Ref. [2] that give the information dimensions for the nonattracting chaotic set and its stable and unstable manifolds in terms of Lyapunov exponents and the decay time, τ . These formulae generalize previous results for nonattracting chaotic sets of two-dimensional maps with one positive and one negative Lyapunov exponent [3, 4], and for Hamiltonian systems of arbitrary dimensionality [5]. In turn, these past results for nonattracting chaotic sets were motivated by the Kaplan-Yorke conjecture which gives the information dimension of a chaotic attractor in terms of its Lyapunov exponents [6]. A rigorous result for the information dimension of an ergodic invariant chaotic set of a two-dimensional diffeomorphism has been given by L.-S. Young [7], and this result supports the Kaplan-Yorke conjecture for attractors and the two-dimensional map results of Refs. [3] and [4] for nonattracting chaotic sets. Furthermore, Ledrappier [8] has proven that the conjectured Kaplan-Yorke dimension formula is an upper bound on the information dimension of chaotic attractors. Soluble examples for typical systems and numerical experiments tend to support the Kaplan-Yorke result. On the other hand, some specific examples violating the Kaplan-Yorke formula also exist. Thus, in the Kaplan-Yorke conjecture they claim that their formula for the dimension applies for "typical" systems. That is, if a specific system

violates the formula then by making a “typical” arbitrarily small change to the system we create a new system for which the Kaplan-Yorke formula holds (this is discussed in Refs. [9] and [10]). Specific systems violating the conjecture are called *atypical*, and, by Ledrappier’s result, have dimensions below the Kaplan-Yorke prediction. The conjectured results of Ref. [2] for nonattracting chaotic sets are also of this character in that they are also claimed to hold only for “typical” systems. Thus, the issue of what constitutes a typical system (or a typical perturbation of an atypical system) is central. At present there is no rigorous formulation of “typical” for this purpose. For this reason it is important to address this question through examples. One of the purposes of this paper is to do just that. More generally, although many examples, both analytical and numerical, exist which support the dimension formula for chaotic attractors, for the case of nonattracting chaotic sets there are virtually no supporting examples (except for the case of two-dimensional maps with one positive and one negative Lyapunov exponent [3, 4]). This paper provides such examples.

In Section 2 we review the results of Ref. [2]. We define the *natural transient measure* on nonattracting chaotic sets and on their stable and unstable manifolds, and give the conjectured information dimension formulae for these measures.

In Section 3 we introduce a noninvertible two-dimensional map with two expanding (positive) Lyapunov exponents. This map is simple enough that it can be fully analyzed. This analysis is especially useful in elucidating certain aspects of the general problem, particularly in relation to the natural transient measure and the role of fluctuation in the finite time Lyapunov exponents.

In Section 4 we introduce our main example, a hard walled billiard chaotic scattering system in three spatial dimensions. For a particular symmetric configuration of the scatterer, we find (Secs. 5 and 6) that the situation is atypical (i.e., the conjectured formula does not apply), but that deviation of the configuration from the symmetric case immediately restores the validity of the conjectured dimension formula.

Section 5 presents numerical results for the dimension in the atypical (symmetric) and typical (asymmetric) cases obtaining good agreement with theoretical results in both cases.

Section 6 gives a theory for the structure of the nonattracting chaotic invariant set present in examples modeling our billiard scatterer. It is shown that the stable manifold of the invariant set is a continuous, nowhere-differentiable surface in both the typical and the atypical cases. Furthermore, we are able to obtain an explicit formula for the dimension in the atypical case (this formula is compared to numerical computations in Sec. 5).

In Sec. 7.1 we present a derivation of the dimension formulae of Sec. 2. Although these formulae have been previously derived in Ref. [2], the previous derivation assumed a specific type of mapping. The situation envisioned in Ref. [2] does not apply to our billiard example. Thus, we are motivated to provide more general arguments for the applicability of the formulae in Sec. 2. In Sec. 7.2 we derive a formula for the dimension of the stable manifold of the chaotic repeller found in the typical (asymmetric) case. This derivation shows

explicitly where the derivation of the typical formula fails for this nontrivial atypical system.

In Sec. 8 we present conclusions and further discussion. In particular, we point out that the continuous, nowhere-differentiable surface forming the stable manifold of our billiard example may be amenable to experimental observation in a situation where the billiard walls are mirrors and the orbits are light rays. In general, we comment that we believe that such optical billiard experiments provide a particularly convenient arena for the experimental investigation of different types of fractal basin boundaries. This has so far proven to be very difficult in other experimental settings.

2 Dimension Formulae

A *chaotic saddle*, Λ , is a *nonattracting*, ergodic, *invariant* set. By *invariant* we mean that all forward and reverse time evolutions of points in Λ are also in Λ . The *stable manifold* of Λ is the set of all initial conditions which converge to Λ upon forward time evolution. The *unstable manifold* of Λ is the set of all initial conditions which converge to Λ upon reverse time evolution. We say Λ is *nonattracting* if it does not completely contain its unstable manifold. In such a case there are points not in Λ that converge to it on backwards iteration.

To define the characteristic escape time, τ , first define a bounded region, R , which contains Λ and no other chaotic saddle. Uniformly sprinkle a large number, $N(0)$, of initial conditions in R . (In this section we take the dynamical system to be a discrete time system, i.e., a map.) Iterate the sprinkled initial conditions forward $n \gg 1$ times and discard all orbits which are no longer in R . Denote the remaining number of orbits $N(n)$. We define τ as

$$e^{-n/\tau} \sim \frac{N(n)}{N(0)}, \quad (3)$$

or, more formally, $\tau = \lim_{n \rightarrow \infty} \lim_{N(0) \rightarrow \infty} \ln[N(0)/N(n)]/n$. The Lyapunov exponents are defined with respect to the *natural transient measure* of the chaotic saddle [11]. This measure is defined on an open set $C \subset R$ as

$$\mu(C) = \lim_{n \rightarrow \infty} \lim_{N(0) \rightarrow \infty} \frac{N(\xi n, n, C)}{N(n)}, \quad (4)$$

where $0 < \xi < 1$, and $N(m, n, C)$ is the number of sprinkled orbits still in R at time n that are also in C at the earlier time $m < n$. The above definition of $\mu(C)$ is presumed to be independent of the choice of ξ as long as $0 < \xi < 1$ (e.g., $\xi = 1/2$ will do).

We take the system to be M -dimensional with U positive and S negative Lyapunov exponents measured with respect to μ (where $U + S = M$) which we label according to the convention,

$$h_U^+ \geq h_{U-1}^+ \geq \dots \geq h_1^+ > 0 > -h_1^- \geq \dots \geq -h_{S-1}^- \geq -h_S^-.$$

Following [2] we define a forward entropy,

$$H = \sum_{i=1}^U h_i^+ - \tau^{-1}.$$

We now define a natural transient measure μ_S on the stable manifold and a natural transient measure μ_U on the unstable manifold. Using the notation of Eq. (4),

$$\mu_S(C) = \lim_{n \rightarrow \infty} \lim_{N(0) \rightarrow \infty} \frac{N(0, n, C)}{N(n)}, \quad (5)$$

$$\mu_U(C) = \lim_{n \rightarrow \infty} \lim_{N(0) \rightarrow \infty} \frac{N(n, n, C)}{N(n)}. \quad (6)$$

Thus, considering the $N(n)$ orbits that remain in R up to time n , the fraction of those orbits that initially started in C gives $\mu_S(C)$, and the fraction that end up in C at the final time n gives $\mu_U(C)$. We use the measure (4), (5), (6) to define the information dimensions of the invariant set, the stable manifold, and the unstable manifold, respectively.

According to Ref. [2], the dimension of the unstable manifold is then

$$D_U = U + I + \frac{H - (h_1^- + \dots + h_I^-)}{h_{I+1}^-}, \quad (7)$$

where I is defined by

$$h_1^- + \dots + h_I^- + h_{I+1}^- \geq H \geq h_1^- + \dots + h_I^-.$$

The dimension of the stable manifold is [2]

$$D_S = S + J + \frac{H - (h_1^+ + \dots + h_J^+)}{h_{J+1}^+}, \quad (8)$$

where J is defined by

$$h_1^+ + \dots + h_J^+ + h_{J+1}^+ \geq H \geq h_1^+ + \dots + h_J^+.$$

Considering the chaotic saddle to be the (generic) intersection of its stable and unstable manifolds, the generic intersection formula gives the dimension of the saddle,

$$D_\Lambda = D_U + D_S - M. \quad (9)$$

It is of interest to discuss some special cases of Eqs. (7)–(9). In the case of a chaotic attractor, the invariant set is the attractor itself, the stable manifold is the basin of attraction, and we identify the unstable manifold with the attractor. Thus $D_S = M$ and $D_\Lambda = D_U$. Since points near the attractor never leave, we have $\tau = \infty$. Equation (7) then yields the Kaplan-Yorke formula [6],

$$D_\Lambda = U + I + \frac{(h_1^+ + \dots + h_U^+) - (h_1^- + \dots + h_I^-)}{h_{I+1}^-}, \quad (10)$$

where I is the largest integer for which $(h_1^+ + \dots + h_U^+) - (h_1^- + \dots + h_I^-)$ is positive.

In the case of a two-dimensional map with one positive Lyapunov exponent h_1^+ and one negative Lyapunov exponent h_1^- with the exponents satisfying $h_1^+ - h_1^- - 1/\tau \leq 0$, Eqs. (7) and (8) give the result of Ref. [3] and [4],

$$D_U = 1 + \frac{h_1^+ - 1/\tau}{h_1^-},$$

$$D_S = 1 + \frac{h_1^+ - 1/\tau}{h_1^+}.$$

Another case is that of a nonattracting chaotic invariant set of a one-dimensional map. In this case $S = 0$ and $U = 1$. The unstable manifold of the invariant set has dimension one, $D_U = 1$. Recalling the definition of the stable manifold as the set of points that approach the invariant set as time increases, we can identify the stable manifold with the invariant set itself. This is because points in the neighborhood of the invariant set are repelled by it unless they lie precisely on the invariant set. Thus, $D_S = D_\Lambda$, and from (8) and (9) we have $D_S = D_\Lambda = H/h_1^+$, where $H = h_1^+ - 1/\tau$.

Still another simple situation is the case of a two-dimensional map with two positive Lyapunov exponents. This case is particularly interesting because we will be able to use it (Sec. 3) to gain understanding of the nature of the natural measure whose dimension we are calculating. In this case $U = 2$ and $S = 0$. Thus $D_U = 2$ and $D_S = D_\Lambda$. There are two cases [corresponding to $J = 0$ and $J = 1$ in Eq. (7)]. For $h_2^+ \tau \leq 1$, we have that $D_S = D_\Lambda$ is between zero and one,

$$D_S = D_\Lambda = 1 + \frac{h_2^+}{h_1^+} - \frac{1}{h_1^+ \tau}. \quad (11)$$

For $h_2^+ \tau \geq 1$, we have that $D_S = D_\Lambda$ is between one and two,

$$D_S = D_\Lambda = 2 - \frac{1}{h_2^+ \tau}. \quad (12)$$

In the next section we will be concerned with testing and illustrating Eqs. (11) and (12) by use of a simple model.

3 Illustrative Expanding Two-Dimensional Map Model

We consider the following example,

$$x_{n+1} = 2x_n \text{ modulo } 1, \quad (13)$$

$$y_{n+1} = \lambda(x_n)y_n + \frac{\eta}{2\pi} \sin(2\pi x_n), \quad (14)$$

where $\lambda(x) > 1$, and the map is defined on the cylinder $-\infty \leq y \leq +\infty$, $1 \geq x \geq 0$, with x regarded as angle-like. We take $\lambda(x)$ to be the piecewise constant function,

$$\lambda(x) = \begin{cases} \lambda_1 & 0 < x < 1/2, \\ \lambda_2 & 1/2 < x < 1, \end{cases} \quad (15)$$

and, without loss of generality, we assume $\lambda_1 \leq \lambda_2$. [Later, in Sec. 3.5, we will consider the problem with a general function $\lambda(x)$ and a general chaotic map $x_{n+1} = M(x_n)$ replacing (13), but for now we focus on (13)–(15).]

For this map, almost every initial condition generates an orbit that either tends toward $y = +\infty$ or toward $y = -\infty$. Figure 1 shows the regions where initial conditions generate these two outcomes, with the black (white) region corresponding to orbits that tend toward $y = -\infty$ ($y = +\infty$). Initial conditions on the border of these two regions stay on the border forever. Thus, the border is an invariant set. It is also ergodic by virtue of the ergodicity of the map $x_{n+1} = 2x_n \bmod 1$. We wish to apply Eqs. (11) and (12) to this invariant set and its natural measure.

The Jacobian matrix for our model is

$$\mathcal{J}(x) = \begin{bmatrix} 2 & 0 \\ \eta \cos 2\pi x & \lambda(x) \end{bmatrix}.$$

Thus, for an ergodic invariant measure of the map, the two Lyapunov exponents are

$$h_a = p \ln \lambda_1 + (1 - p) \ln \lambda_2 \quad (16)$$

and

$$h_b = \ln 2,$$

where p is the measure of the region $x < 1/2$. To find h_a we thus need to know the measure of the invariant set. The measure we are concerned with is the natural transient measure introduced in Sec. 2.

3.1 The Decay Time and the Natural Measure

Consider a vertical line segment of length ℓ_0 whose x coordinate is x_0 and whose center is at $y = y_0$. After one iterate of the map (13)–(15), this line segment will have length $\ell_1 = \lambda(x_0)\ell_0$ and be located at $x = x_1$ with its center at $y = y_1$, where (x_1, y_1) are the iterates of (x_0, y_0) using the map (13)–(15). Thus we see that vertical line segments are expanded by the multiplicative factor $\lambda(x) \geq \lambda_1 > 1$. Now consider the strip, $-K \leq y \leq K$, and sprinkle many initial conditions uniformly in this region with density ρ_0 . A vertical line segment, $x = x_0$, $-K \leq y \leq K$, iterates to $x = x_1$ and with its center at $y_1 = (\eta/2\pi) \sin 2\pi x_0$. We choose $K > (\eta/2\pi)(\lambda_1 - 1)^{-1}$ so that the iterated line segment spans the strip $-K \leq y \leq K$. After one iterate, the density will still be uniform in the strip: The region $x < 1/2$ ($x > 1/2$), $-K \leq y \leq K$, is expanded uniformly vertically by λ_1 (λ_2) and horizontally by 2. Thus, after one iterate,

the new density in the strip is $\rho_1 = [(\lambda_1^{-1} + \lambda_2^{-1})/2]\rho_0$, and, after n iterates, we have

$$\rho_n = [(\lambda_1^{-1} + \lambda_2^{-1})/2]^n \rho_0.$$

Hence the exponential decay time for the number of orbits remaining in the strip is

$$\frac{1}{\tau} = \ln \left[\frac{1}{2} \left(\frac{1}{\lambda_1} + \frac{1}{\lambda_2} \right) \right]^{-1}. \quad (17)$$

To find the natural stable manifold transient measure of any x -interval $s_m^{(n)} = [m/2^n, (m+1)/2^n]$, where $m = 0, 1, \dots, 2^n - 1$, we ask what fraction of the orbits that were originally sprinkled in the strip and are still in the strip at time n started in this interval. Let $s_m^{(n)}$ experience $n_1(m)$ vertical stretches by λ_1 and $n_2(m) = n - n_1(m)$ vertical stretches by λ_2 . Then the initial subregion of the $s_m^{(n)}$ still in the strip after n iterates has vertical height $K \lambda_1^{-n_1(m)} \lambda_2^{-n_2(m)}$. Hence the natural measure of $s_m^{(n)}$ is

$$\mu(s_m^{(n)}) = \frac{2^{-n} \lambda_1^{-n_1(m)} \lambda_2^{-n_2(m)}}{[\frac{1}{2}(\lambda_1^{-1} + \lambda_2^{-1})]^n} = \frac{\lambda_1^{n_2(m)} \lambda_2^{n_1(m)}}{(\lambda_1 + \lambda_2)^n}. \quad (18)$$

(Note that this is consistent with $\mu([0, 1]) = \sum_{m=0}^{2^n-1} \mu(s_m^{(n)}) = 1$.) Thus the measures of the intervals $[0, 1/2]$ and $[1/2, 1]$ are

$$p = \mu(s_0^{(1)}) = \frac{\lambda_2}{\lambda_1 + \lambda_2}$$

and

$$1 - p = \mu(s_1^{(1)}) = \frac{\lambda_1}{\lambda_1 + \lambda_2}.$$

It is important to note that our natural transient measures p and $(1-p)$ for the two-dimensional map are different from the natural measures of the same x -intervals for the one-dimensional map, $x_{n+1} = 2x_n \bmod 1$, alone. In that case, with probability one, a random choice of x_0 produces an orbit which spends half its time in $[0, 1/2]$ and half its time in $[1/2, 1]$, so that in this case the natural measures of these regions are $p = (1-p) = 1/2$. The addition of the y -dynamics changes the natural measure of x -intervals.

From (16) we obtain

$$h_a = \frac{\lambda_2}{\lambda_1 + \lambda_2} \ln \lambda_1 + \frac{\lambda_1}{\lambda_1 + \lambda_2} \ln \lambda_2. \quad (19)$$

For a general function $f(Z)$ with $d^2 f/dZ^2 < 0$, averaging over different values of Z gives the well-known inequality $\langle f(Z) \rangle \leq f(\langle Z \rangle)$ where $\langle (\dots) \rangle$ denotes the average of the quantity (\dots) . Using $f(Z) = \ln Z$ with $Z = \lambda_1$ with probability $p = \lambda_2/(\lambda_1 + \lambda_2)$ and $Z = \lambda_2$ with probability $(1-p)$, this inequality and Eqs. (17) and (19) yield the result that

$$h_a \leq \frac{1}{\tau}. \quad (20)$$

In fact, we will see in Sec. 3.5 that (20) remains true for any choice of the function $\lambda(x) > 1$ in (14). In (20) the equality sign applies if the vertical stretching is uniform ($\lambda_1 = \lambda_2$) but, for any nonuniformity in the vertical stretching ($\lambda_1 \neq \lambda_2$), h_a is strictly less than $1/\tau$.

3.2 Application of the Dimension Formulae

Let $\lambda_2 = r\lambda_1$, $r > 1$, and imagine that we fix r and vary λ_1 . Applying Eqs. (11) and (12) to our example we obtain three cases,

- (a) $h_b > 1/\tau > h_a$ (λ_1 small),
- (b) $1/\tau > h_b > h_a$ (λ_1 moderate), and
- (c) $1/\tau > h_a > h_b$ (λ_1 large).

Corresponding to these three cases (11) and (12) yield the following values for D_Λ , the dimension of the invariant set,

$$D_a = 1 + \frac{\ln(1+r^{-1}) - \ln \lambda_1}{\ln 2}, \text{ for } \lambda_1 \leq \lambda_a, \quad (21)$$

$$D_b = \frac{\ln(1+r^{-1}) + (1+r)^{-1} \ln r}{\ln \lambda_1 + (1+r)^{-1} \ln r}, \text{ for } \lambda_a \leq \lambda_1 \leq \lambda_b, \quad (22)$$

$$D_c = \frac{\ln(1+r^{-1}) + (1+r)^{-1} \ln r}{\ln 2}, \text{ for } \lambda_b \leq \lambda_1, \quad (23)$$

where $\ln \lambda_a = \ln(1+r^{-1})$ and $\ln \lambda_b = \ln 2 - (1+r)^{-1} \ln r$. The solid line in Fig. 2 shows a plot of D_Λ versus $\ln \lambda_1$ for $r = 3$. Note that for large λ_1 , $D_\Lambda = D_c$ is independent of λ_1 .

It is also instructive to consider the case of uniform stretching ($r = 1$) for which $\lambda_1 = \lambda_2$. In that case, $h_a = 1/\tau$, and there is a rigorous known result for the dimension [10]. For $\lambda_1 = \lambda_2$, Eqs. (21)–(23) yield

$$D_\Lambda = \begin{cases} 2 - \frac{\ln \lambda_1}{\ln 2} & \text{for } 1 \leq \lambda_1 \leq 2, \\ 1 & \text{for } \lambda_1 \geq 2. \end{cases} \quad (24)$$

(For $r \rightarrow 1$ region (b), where $D_\Lambda = D_b$, shrinks to zero width in λ_1 .) For $r = 1$ the natural transient measure is uniform; from (18) we have $\mu(s_m^{(n)}) = 2^{-n}$ independent of the interval (i.e, independent of m). In this case there is no difference between the capacity dimension of the invariant set and the information dimension of its measure. Equation (24) agrees with the rigorous known result, thus lending support to the original conjecture.

3.3 Numerical Tests

The formulae (21)–(23) were verified by numerical measurements of the information dimension, D_1 , of Λ at various values of λ_1 with $r = \lambda_2/\lambda_1$ fixed at $r = 3$ (Fig. 2). Shown for comparison is the box-counting dimension, D_0 . The values of the box-counting dimension are numerically indistinguishable from the

values of the information dimension when D_0 , $D_1 > 1$, or $\lambda_1 < \lambda_a$, the region corresponding to formula (21). For $\lambda_1 > \lambda_a$, Λ is a smooth curve and so has a box-counting dimension of $D_0 = 1$. No points for D_1 are shown near $\lambda_1 = \lambda_b$. It can be argued (Appendix A) that numerical convergence is too slow here to yield accurate measurements of the dimension.

To numerically determine the information dimension of Λ (the data shown as open squares in Fig. 2), we place a square $x-y$ grid with a spacing ε between grid points over a region containing Λ . Using the method described in the next paragraph we compute the natural measure in each grid box and repeat for various ε . The information dimension is then given by

$$D_1 = \lim_{\varepsilon \rightarrow 0} \frac{I(\varepsilon)}{\ln(1/\varepsilon)},$$

where $I(\varepsilon) = \sum_{i=1}^{N(\varepsilon)} \mu_i \ln(1/\mu_i)$ is a sum over the $N(\varepsilon)$ grid boxes which intersect Λ and μ_i is the natural measure in the i th box. The slope of a plot of $I(\varepsilon)$ versus $\ln \varepsilon$ gives D_1 . The box-counting dimension (the data shown as black dots in Fig. 2) is given by

$$D_0 = \lim_{\varepsilon \rightarrow 0} \frac{\ln N(\varepsilon)}{\ln 1/\varepsilon}$$

and calculated in an analogous way.

To determine which boxes intersect Λ and what measure is contained in each of them we take advantage of the fact that Λ is a function [11] [see Appendix A, Eq. (A2)]. That is, for each value of x there is only one corresponding value of y in Λ , which we denote $y = y_\Lambda(x)$. We divide the interval $0 \leq x < 1$ into 2^n intervals of width $\delta \equiv 2^{-n}$. We wish to approximate $y_\Lambda(x_0)$ for x_0 in the center of the x -interval. To do this we iterate x_0 forward using (13) m times until the condition

$$\frac{\delta}{2} \lambda_1^{m_1} \lambda_2^{m_2} \geq 1 \tag{25}$$

is first met, where m_1 (m_2) is the number of times the orbit lands in $0 \leq x < 1/2$ ($1/2 \leq x < 1$), and $m_1 + m_2 = m$ (we will see the reason for this condition below). All of the values, x_i , of the iterates are saved. Starting now from x_m and taking $y_m = 0$ we iterate backward m times. For η small enough, Λ is contained in $-1 \leq y \leq 1$, so the point $(x_m, y_m = 0)$ is within a distance 1 in the y -direction of Λ . The m reverse iterations shrink the segment $y_m \leq y \leq y_\Lambda(x_m)$ by a factor $\lambda_1^{m_1} \lambda_2^{m_2}$ so that $|y_0 - y_\Lambda(x_0)| \leq \delta/2$ by condition (25). Thus, we have found a point y_0 that approximates $y_\Lambda(x_0)$ to within δ . Since we will be using ε boxes with $\varepsilon \gg \delta$, we may regard y_0 as being essentially equal to $y_\Lambda(x_0)$. The measure in the δ width interval containing x_0 is found by iterating x_0 forward n times and using equation (18), $\mu = \frac{\lambda_1^{n_2} \lambda_2^{n_1}}{(\lambda_1 + \lambda_2)^n}$, where n_1 (n_2) is the number of times the orbit lands in $0 \leq x < 1/2$ ($1/2 \leq x < 1$), and $n_1 + n_2 = n$. We associate this measure with the point (x_0, y_0) (with y_0 found by the above procedure).

Note that for fractal $y_\Lambda(x)$ the y interval occupied by the curve $y = y_\Lambda(x)$ in an x interval of width $\delta \ll 1$ is of order δ^{D_0-1} which is large compared to δ . We now cover the region with new grids having successively larger spacing, $\varepsilon_i = 2^i \delta = 2^{i-n}$, and calculate $I(\varepsilon_i)$ and $N(\varepsilon_i)$ based on the data taken from the first δ -grid. For i large enough, such that the y extent of the curve $y_\Lambda(x)$ in a typical δ width interval is less than ε_i (i.e., $\varepsilon_i \gtrsim \delta^{2-D_0}$ or $i \gtrsim (D_0 - 1)n$) we observe linear scaling of $\log I(\varepsilon_i)$ and $\log N(\varepsilon_i)$ with $\log \varepsilon_i$, and we use the slope of such plots to determine D_1 and D_0 . The dimensions D_1 and D_0 are then determined as described above.

3.4 Atypical Case

The conjecture of Ref. [2] is that the dimension formulae of Sec. 2 apply for “typical” systems. To see the need for this restriction consider Eqs. (14) for the case where $\eta = 0$. It is easily shown that the dimension formulae can be violated in this case. The claim, however, is that $\eta = 0$ is special, or “atypical”, in that, as soon as we give η any nonzero value, the validity of the dimension formulae is restored. In this connection it is important to note that as long as $\eta \neq 0$, the dimension of the invariant set is independent of the value of η . This follows since if $\eta \neq 0$ we can always rescale the value of η to one by the change of variables $\tilde{y} = y/\eta$. To see the violation of the dimension formulae for $\eta = 0$, we note that in this case, by virtue of (14), the line $y = 0$ is invariant. Thus the measure is distributed on a one-dimensional subspace, the x -axis. (This is very different from the picture in Fig. 1, where the invariant set, the boundary between black and white, appears to be fractal.) Using the definition of the information dimension and dividing the x -axis into intervals of width 2^{-n} , the information dimension of the natural measure is

$$D_\Lambda = \lim_{n \rightarrow \infty} \frac{\sum_{m=0}^{n-1} \mu(s_m^{(n)}) \ln[1/\mu(s_m^{(n)})]}{\ln(2^n)}. \quad (26)$$

The quantity whose limit is taken in (26) is in fact independent of n . Thus, taking $n = 1$ we obtain for D_Λ the result that, for $\eta = 0$,

$$D_\Lambda = D_c,$$

for all λ_1 and $\lambda_2 > 1$, where D_c is given by (23). Thus, for $h_a < h_b$, D_Λ is greater when $\eta \neq 0$ than when $\eta = 0$, and, thus, the conjectured stable manifold dimension formula of Sec. 2 is violated. For $h_a > h_b$, D_Λ is the same in both cases.

In Sec. 4 we consider chaotic scattering in a three-dimensional billiard example for which the character of the atypical case is more interesting than in the above example. In particular, we find for our billiard that in both the typical and the atypical cases the stable manifold can have noninteger capacity dimension.

3.5 General Considerations

The previous considerations readily generalize to the case of an arbitrary smooth function $\lambda(x) > 1$ and a general chaotic map, $x_{n+1} = M(x_n)$, which replaces (3.1). Consider the finite time vertical Lyapunov exponent,

$$\tilde{h}(x, n) = \frac{1}{n} \sum_{m=1}^n \ln \lambda(M^{m-1}(x))$$

computed for the initial condition x . Choosing x randomly with uniform probability distribution in the relevant basin for chaotic motion [e.g., x in $[0, 1]$ for Eq. (13)], $\tilde{h}(x, n)$ can be regarded as a random variable. Let $\tilde{P}(h, n)$ denote its probability distribution function. For large n , we invoke large deviation theory to write $\tilde{P}(h, n)$ as [11]

$$\ln \tilde{P}(h, n) = -nG(h) + o(n),$$

or, more informally,

$$\tilde{P}(h, n) \sim e^{-nG(h)}, \quad (27)$$

where the specific form of $G(h)$ depends on $M(x)$ and the specific $\lambda(x)$, and $G(h)$ is convex, $d^2G(h)/dh^2 \geq 0$. For the normalization, $\int \tilde{P}(h, n)dh = 1$, to hold for $n \rightarrow \infty$, we have that

$$\min_h G(h) = 0;$$

see Fig. 3, where \bar{h} denotes the value of h for which the above minimum is attained. As $n \rightarrow \infty$ we see that \tilde{P} approaches a delta function, $\delta(h - \bar{h})$. Thus, \bar{h} is the usual infinite time Lyapunov exponent for almost all initial conditions with respect to Lebesgue measure in $0 \leq x \leq 1$.

As described above $\tilde{P}(h, n)$ is the probability distribution of $h(x, n)$ for x chosen randomly with respect to a uniform distribution in $[0, 1]$. We now ask what the probability distribution of $h(x, n)$ is for x chosen randomly with respect to the natural transient measure for our expanding map, $x_{n+1} = M(x_n)$ and (14). To answer this question we proceed as before and consider an initial vertical line segment $|y| \leq K$ starting at x [with $K > (\eta/2\pi)(\lambda_{\min} - 1)^{-1}$, $\lambda_{\min} = \min_x \lambda(x) > 1$]. After n iterations, this line segment lengthens by the factor $\exp[n\tilde{h}(x, n)]$. Thus, the fraction of the line still remaining in the strip $|y| < K$ is $\exp[-n\tilde{h}(x, n)]$. Hence, the fraction of points sprinkled uniformly in the strip that still remains after n iterates is

$$e^{-n/\tau} \sim \int e^{-nG(h) - nh} dh, \quad (28)$$

and the probability distribution of finite time vertical Lyapunov exponents for x chosen randomly with respect to the natural transient measure is

$$P(h, n) \sim \frac{e^{-nG(h) - nh}}{\int e^{-nG(h) - nh} dh}. \quad (29)$$

Evaluating (28) for large n we have $\int e^{-n[G(h)+h]}dh \sim e^{-n[G(h_*)+h_]}$, where $\min[G(h)+h] = G(h_*)+h_*$ and h_* is the solution of $dG(h_*)/dh_* = -1$. Thus ,

$$1/\tau = G(h_*) + h_*. \quad (30)$$

See the construction in Fig. 3, in which the dotted line of slope -1 is tangent to the graph of $G(h)$ at the point $h = h_*$. The infinite time vertical Lyapunov exponent for the transient natural measure is

$$h_a = \int hP(h,n)dh. \quad (31)$$

Using (29) and again letting n be large (31) yields $h_a = h_*$. Referring to Fig. 3 we see that

$$h_a \leq 1/\tau.$$

That is, Eq. (20) is valid for general $M(x)$ and $\lambda(x)$ and not just for $M(x)$ and $\lambda(x)$ given by (13) and (15).

4 A Three-Dimensional Billiard Chaotic Scatterer

We consider a three degree-of-freedom billiard. The billiard (Fig. 4) is formed by a hard ellipsoid of revolution, placed in a hard, infinitely long tube with cross-section as shown in Fig. 4(b). The center of the ellipsoid is placed at the center of the tube. We consider two cases: (a) the major axis of the ellipsoid coincides with the z -axis [see Fig 4(a)], (b) the major axis of the ellipsoid lies in the y - z plane and makes an angle ξ with the z -axis. The ratio of the minor radius of the ellipsoid (r_{\parallel}) to the width of a side of the tube [dashed line in Fig. 4(b)] is $1/4$. This leaves the major radius, r_{\perp} , and the tilt angle, ξ , as parameters. A point particle injected into the system experiences specular reflection from the ellipsoid and the walls (i.e., the angle of reflection is equal to the angle of incidence, where both are taken with respect to the normal to the surface off of which the particle bounces). When the orbit has passed the top (bottom) of the ellipsoid, with positive (negative) z -velocity, we say that it has exited upward (downward). We fix the conserved energy so that $|\vec{v}| = 1$.

4.1 Pictures of the Stable Manifold

We claim that the case of the untilted ellipsoid [$\xi = 0$ and case (a) above] is atypical in the sense that it violates the formulae of Sec. 2. However, as soon as $\xi \neq 0$, we claim that the formulae of Sec. 2 apply. We begin by discussing the atypical (untilted) case.

By the symmetry of the geometry of the billiard with the ellipsoid axis along z [Fig. 4(a)], the chaotic saddle, Λ , of this system is the collection of initial conditions satisfying $z = v_z = 0$. Started with these initial conditions, an

orbit will have $z = v_z = 0$ for all forward and reverse time. The surface normals of the ellipsoid and walls at $z = 0$ lie in the $z = 0$ plane, and thus the particle cannot acquire a non-zero v_z . The $z = 0$ slice through the three-dimensional billiard is a two-dimensional billiard with concave walls [Fig. 4(b)]. It is known [11] that a typical orbit in this billiard will fill the phase space ergodically. Near $z = 0$, we can picture a typical point on the stable manifold (denoted SM) as having, for example, z slightly less than zero and v_z slightly greater than zero. The particle will hit the ellipsoid below its equator and, thus, v_z will be decreased with each bounce, yet remain positive. With successive bounces, the orbit on SM slowly approaches $z = v_z = 0$, the chaotic saddle.

To visualize SM , we note that it forms the boundary between initial conditions which escape upward and those which escape downward. We say that points which, when iterated, eventually escape upward (downward) are in the *basin* of upward (downward) escape. Points which are on the boundary between the two basins never escape at all, i.e. they are in SM . We initiate a (two-dimensional) grid of orbits (500x500) on the plane, $-3 < x < 3$, $y = 5.1$, $-2.5 < z < 0$, $v_x = 0$, $v_z = .1$, and v_y is given by the condition $|\vec{v}| = 1$. We iterate each of these initial conditions forward until it escapes. Then we plot a white (black) point for each orbit in the upward (downward) basin. The result is shown in Fig. 5(a). The boundary between the white and black regions is then the intersection of SM lying in the phase space of the five-dimensional billiard (x, y, z, v_x, v_y, v_z constrained by $|\vec{v}| = 1$) with the specified two-dimensional x, z -plane. SM appears to take the form of a nowhere-differentiable curve. This is true in various 2D slices, none of which are chosen specially, which suggests that SM has this form in a typical slice. A similar procedure can be followed for the case of the tilted ellipsoid and the resulting picture is shown in Fig. 5(b) for the case of a tilt angle of $\xi = 2\pi/100$ radians.

4.2 Lyapunov Exponents, Decay Times, and Approximate Formulae for the Stable Manifold

Again, we begin with the untilted case. To construct a map from this system we record the cylindrical coordinates (z, ϕ) and their corresponding z and ϕ velocity components, which we denote (v, ω) , each time the particle hits the ellipsoid. The coordinate r is constrained, for a given z , by the shape of the ellipsoid surface, and v_r is given by the energy conservation condition $|\vec{v}| = 1$. The four components $(z, v, \phi, \omega)_n$ give the state of the system at discrete time n , where n labels the number of bounces from the ellipsoid. Let $\vec{z} \equiv \begin{bmatrix} z \\ v \end{bmatrix}$ and $\vec{\phi} \equiv \begin{bmatrix} \phi \\ \omega \end{bmatrix}$. For future reference, we express the map using the following notation,

$$\begin{aligned} \vec{z}_{n+1} &= M_z(\vec{z}_n, \vec{\phi}_n), \\ \vec{\phi}_{n+1} &= M_\phi(\vec{z}_n, \vec{\phi}_n). \end{aligned} \tag{32}$$

In what follows, when we refer to an orbit, saddle, invariant set, stable manifold, etc., we are referring to these quantities for the discrete time map (rather than the original continuous time system).

In the case of the untilted ellipsoid, linearizing about an orbit on Λ , (i.e., $\vec{z}_n = 0, \vec{\phi}_n$), we obtain, for the evolution of differential orbit perturbations $\delta\vec{z}$ and $\delta\vec{\phi}$,

$$\begin{aligned}\delta\vec{z}_{n+1} &= DM_z(0, \vec{\phi}_n)\delta\vec{z}_n, \\ \delta\vec{\phi}_{n+1} &= DM_\phi(0, \vec{\phi}_n)\delta\vec{\phi}_n,\end{aligned}$$

where $\vec{\phi}_{n+1} = M_\phi(0, \vec{\phi}_n)$ is the map for the two-dimensional billiard of Fig. 4(b), $DM_z(0, \vec{\phi})$ is the tangent map for differential orbit perturbations in \vec{z} evaluated at $\vec{z} = 0$, and $DM_\phi(0, \vec{\phi})$ is the tangent map for differential perturbations lying in Λ . Let $\pm h_z$ and $\pm h_\phi$ denote the Lyapunov exponents with respect to the *natural transient measure* (Sec. 2) for perturbations in \vec{z} and in $\vec{\phi}$, respectively (these exponents occur in positive-negative pairs due to the Hamiltonian nature of the problem).

In principle, one could numerically evaluate h_z and h_ϕ by sprinkling a large number, N , of initial conditions in the vicinity of Λ , iterating $n \gg 1$ times, evaluating h_z and h_ϕ over those orbits still near Λ , and averaging h_z and h_ϕ over those orbits. We could also find τ by this procedure; it is the exponential rate of decay of the orbits from the vicinity of Λ . For cases where the escape time τ is not long, this procedure, however, becomes problematic. For finite N the number of retained orbits can be small or zero if n is too large. Thus, we adopt an alternate procedure which we found to be less numerically demanding.

In particular we make use of the ideas presented in Sec. 3.5. We define the *uniform measure* as the measure generated by uniformly sprinkling many initial conditions in Λ (the hyperplane $z = v_z = 0$). An average over these orbits of the tangent space stretching exponents would yield uniform measure Lyapunov exponents. We denote the distribution of finite-time Lyapunov exponents with respect to this measure by $P(\tilde{h}_\phi, \tilde{h}_z, n) \sim e^{-nG(\tilde{h}_\phi, \tilde{h}_z)}$ [as in Eq. (27)], where the tilde indicates finite time exponents for initial conditions distributed according to the uniform measure.

To compute the decay time and the Lyapunov exponents with respect to the natural transient measure we note that orbits near a point $\vec{\phi}$ in Λ iterate away from Λ as $\exp[n\tilde{h}_z(\vec{\phi}, n)]$. Thus, the fraction of a large number of initial conditions sprinkled near Λ which remain near Λ after n iterates is

$$\int P(\tilde{h}_\phi, \tilde{h}_z, n) e^{-n\tilde{h}_z} d\tilde{h}_z,$$

and h_ϕ (the infinite time Lyapunov exponent with respect to the natural transient measure) is

$$h_\phi = \lim_{n \rightarrow \infty} \frac{\int \tilde{h}_\phi P(\tilde{h}_\phi, \tilde{h}_z, n) e^{-n\tilde{h}_z} d\tilde{h}_z}{\int P(\tilde{h}_\phi, \tilde{h}_z, n) e^{-n\tilde{h}_z} d\tilde{h}_z}.$$

This expression can be approximated numerically by choosing N initial conditions, $\vec{\phi}_i$, uniformly in Λ and calculating

$$\langle n\tilde{h}_\phi \rangle_n \equiv \frac{n \sum_{i=1}^N \tilde{h}_\phi(\vec{\phi}_i, n) e^{-n\tilde{h}_z(\vec{\phi}_i, n)}}{N \sum_{i=1}^N e^{-n\tilde{h}_z(\vec{\phi}_i, n)}}.$$

We calculate the finite-time Lyapunov exponents $\tilde{h}_\phi(\vec{\phi}_i, n)$ and $\tilde{h}_z(\vec{\phi}_i, n)$ using the QR decomposition method [18]. Since we chose the $\vec{\phi}_i$ uniformly in Λ these exponents are distributed according to $P(n, \tilde{h}_\phi, \tilde{h}_z)$. N is taken to be large enough that there are at least 100 terms contributing to 90% of each sum. The range of n is from 10 to about 40. We find that $\langle n\tilde{h}_\phi \rangle_n$ versus n is well-fitted by a straight line and we take its slope as our estimate of h_ϕ .

To find τ , first note that we numerically find that h_ϕ does not vary much from \bar{h}_ϕ ($.91 \leq h_\phi/\bar{h}_\phi \leq 1$) as we change the system parameter (the height of the ellipsoid), where the overbar denotes an infinite-time Lyapunov exponent with respect to the uniform measure on Λ . Thus, we make the approximation $P(\tilde{h}_\phi, \tilde{h}_z, n) \approx P(\tilde{h}_z, n)$, $G(\tilde{h}_\phi, \tilde{h}_z) \approx G(\tilde{h}_z)$ and plot $G(\tilde{h}_z)$ versus \tilde{h}_z . The value of $1/\tau$ is given by Eq. (30), and h_z is given by $dG(n, h_z)/d\tilde{h}_z = -1$. (Note that $h_z \leq 1/\tau \leq \bar{h}_z$.) A third order polynomial is fit to the data for $G(\tilde{h}_z)$ and used to find τ and h_z . This calculation is performed at a value of n which allows a significant number of points in $G(\tilde{h}_z)$ versus \tilde{h}_z to be collected near in the range $h_z < \tilde{h}_z < \bar{h}_z$.

For the case of the tilted ellipsoid, we will consider a very small tilt angle, $\xi = 2\pi/100$. With this small tilt angle, the Lyapunov exponents and decay times for the tilted and the untilted cases are approximately the same. Thus, for the tilted case, we will use the same Lyapunov exponent values, $\pm h_z$ and $\pm h_\phi$ and decay time τ , that we numerically calculated for the untilted case. The dimension formula of Sec. 2 for SM is

$$\begin{aligned} D_S &= 4 - (h_\phi\tau)^{-1} && \text{for } h_\phi\tau \geq 1, \\ D_S &< 3 && \text{for } h_\phi\tau < 1. \end{aligned} \quad (33)$$

(As for cases (b) and (c) of Sec. 3.2, we could write explicit expressions for D_S for $h_\phi\tau < 1$, but, in what follows we only need that $D_S < 3$ in this case.)

If the tilt angle is made to be zero ($\xi = 0$), we find that D_S is not given by (33), but by the following formula (which we derive in Sec. 7.2),

$$\begin{aligned} D_S &= 4 - \frac{h_z + 1/\tau}{h_\phi} && \text{for } h_\phi \geq h_z + 1/\tau, \\ D_S &< 3 && \text{for } h_\phi < h_z + 1/\tau. \end{aligned} \quad (34)$$

Since D_S is given by (34) only if the tilt angle ξ is precisely zero, we say that the untilted ellipsoid scattering system is atypical. As conjectured in [2], D_S from (33) is greater than or equal to D_S from (34). Note that D_S from the first line of (33) is larger than D_S from the first line of (34) by the factor h_z/h_ϕ . Although the transition of D_S from $\xi = 0$ to $\xi \neq 0$ is strictly discontinuous, there is also a continuous aspect: In numerically calculating the dimension of

a measure one typically plots $\ln I(\epsilon)$ versus $\ln(1/\epsilon)$, where $I(\epsilon) = \sum \mu_i \ln[1/\mu_i]$ and μ_i is the measure of the i^{th} cube in an ϵ grid. One then estimates the dimension as the slope of a line fitted to small ϵ values in such a plot. In the case of very small tilt, such a plot is expected to yield a slope given by (34) for $\epsilon \gtrsim \epsilon_*$ and subsequently, for $\epsilon \lesssim \epsilon_*$, to yield a slope given by (33). Here ϵ_* is a small tilt-dependent cross-over value, where $\epsilon_* \rightarrow 0$ as $\xi \rightarrow 0$. In such a case, the dimension, which is defined by the $\epsilon \rightarrow 0$ limit, is given by (33).

5 Numerical Computations for the Three-Dimensional Billiard Scatterer

To verify that the untilted system is atypical we numerically calculated the box-counting dimension of SM for various values of the parameter r_\perp , then introduced a small tilt perturbation in the form of a $-2\pi/100$ radian tilt of the ellipsoid about the x -axis and repeated the dimension calculations. The results are shown in Fig. 6. They confirm Eqs. (33) and (34). (We do not plot data points near the kink in the theoretical curve because of the numerical difficulty in obtaining reliable results in that parameter range. This is a result of slow converge near the kink. It is also found in the example of Sec. 3.3 and discussed in Appendix A.)

We compare measured values of the box-counting dimension to the predicted values of the information dimension in Fig. 6. The box-counting dimension gives an upper bound on the information dimension, but often the values of the two dimensions are very close. In particular, we can compare the result for the tilted ellipsoid system to the 2D map of Sec. 3. In the regime $h_\phi \geq 1/\tau$, our system is similar to case (a) studied in Section 3.2 (note that, as discussed in Sec. 4, $1/\tau$ is never smaller than h_z). Changing r_\perp while leaving r_\parallel fixed changes τ while h_ϕ changes only slightly. This is similar to varying λ_1 of the 2D map while keeping λ_2 fixed, i.e. varying r . Figure 2, shows (for a particular value of r) that the measured values of D_0 and D_1 are numerically indistinguishable in the region corresponding to case (a), $\lambda < \lambda_a$.

For $h_\phi\tau < 1$ ($h_\phi < h_z + 1/\tau$) the information dimension of SM is predicted to be less than three for the tilted (untilted) ellipsoid system. This is analogous to cases (b) and (c) of Sec. 3.2; see Fig. 2. Since SM divides the four-dimensional phase space, its box-counting dimension cannot be less than three, and, analogous to the result of Sec. 3 and Fig. 2, we expect that the box-counting dimension is three for $h_\phi\tau < 1$ ($h_\phi < h_z + 1/\tau$). This expectation is borne out by the numerical results, Fig. 6.

The box-counting dimension of SM was computed using the uncertainty dimension method [1, 11]. This method gives the box-counting dimension of the basin boundary which, as discussed above, coincides with SM .

The uncertainty dimension method was carried out as follows:

1. Choose a point, \vec{x} , at random in a region of a 2D plane intersecting the

basin boundary (e.g., Fig. 6) and determine by iteration in which basin it lies.

2. Determine in which basins the perturbed initial points $\vec{x} \pm \vec{\delta}$ lie ($\vec{\delta}$ is some small vector).
3. If the three points examined in (1) and (2) do not all lie in the same basin, then \vec{x} is called “uncertain”.
4. Repeat 1 to 3 for many points \vec{x} randomly chosen in the 2D plane, and obtain the fraction of these that are uncertain.
5. The fraction of points which is uncertain for a given $\vec{\delta}$, denoted f , scales like [12] $f \sim |\vec{\delta}|^{2-d_0}$, where d_0 is the box-counting dimension of the intersection of SM with the 2D plane. The box-counting dimension of SM in the full 4D state space of the map is $D_0 = 2 + d_0$. (The dimension of a generic intersection of a 2D plane with a set having dimension D_0 in a 4D space is $d_0 = 2 + D_0 - 4$, which gives $D_0 = 2 + d_0$.) Thus, plot $\ln f$ versus $\ln |\vec{\delta}|$, fit a straight line to the plot, and estimate D_0 as 4 minus the slope of this line. See Fig. 8 for an example of such a plot.

6 Structure of the Stable Manifold

6.1 Untilted Ellipsoid

Due to the symmetry to the untilted ellipsoid billiard, the chaotic saddle of the untilted ellipsoid system has a special geometry (i.e., it lies in $z = v = 0$), which, as we show, accounts for the dimension being lower than the predicted value for a typical system. Similarly, the symmetry induces a special geometry on the stable manifold (SM). Figure 7 shows a 3D slice of SM in the atypical system. The slice is at a fixed value of ω . The axes are z , v , and ϕ , but one could have chosen an arbitrary line through (ϕ, ω) as the third axes and seen a plot which was qualitatively the same. The stable manifold is organized into rays emanating from the ϕ -axis with oscillations along the ϕ -direction. The magnitude of the oscillations decreases to zero as the ϕ -axis is approached.

To understand the structure of SM in more detail, assume that $|\vec{z}|$ is small. Then, since $|\vec{z}| = 0$ is invariant, we can approximate the dynamics by expanding to first order in \vec{z} ,

$$\vec{z}_{n+1} \cong DM_z(0, \vec{\phi}_n) \vec{z}_n, \quad (35)$$

$$\vec{\phi}_{n+1} \cong M_\phi(0, \vec{\phi}_n). \quad (36)$$

Say $(\vec{z}_{SM}, \vec{\phi}_{SM})$ is a point on SM . As this point is iterated we have that $|\vec{z}| \rightarrow 0$ with increasing n . However, since (35) is linear in \vec{z}_n , for any constant α , and the initial condition, $(\alpha \vec{z}_{SM}, \vec{\phi}_{SM})$, the subsequent orbit must also have $|\vec{z}| \rightarrow 0$. Consequently, if $(\vec{z}_{SM}, \vec{\phi}_{SM})$ lies in SM , so does $(\alpha \vec{z}_{SM}, \vec{\phi}_{SM})$. Thus, for the system (35), (36), the stable manifold at any point $\vec{\phi}$ lies on a straight

line through the origin of the two-dimensional \vec{z} -space. Put another way, in the approximation (35), (36), the stable manifold can be specified by an equation giving the *angle* of \vec{z} as a function of $\vec{\phi}$. Thus, decomposing into polar coordinates (ρ, χ) , the stable manifold for $|\vec{z}| \rightarrow 0$ approaches the form

$$\chi = \chi(\vec{\phi}). \quad (37)$$

(This explains the structure seen in Fig. 7.) For $|\vec{z}|$ finite the linearity of (35) is not exact, and we expect that the behavior of the stable manifold at constant $\vec{\phi}$ is not a straight line through the origin of the \vec{z} plane. Rather, as $|\vec{z}|$ becomes larger we expect (and numerically observe) the straight line for small $|\vec{z}|$ to appear as a smooth curve through $\vec{z} = 0$.

Since for fixed $\vec{\phi}$ SM varies smoothly with increasing $\rho = |\vec{z}|$, the dimension of SM is not affected by the approximation (35) and (36). That is, to find the dimension of SM , we can attempt to find it in the region of small $|\vec{z}|$ where (35) and (36) are valid, and that determination will apply to the whole of SM .

The task of analytically determining D_S is too hard for us to accomplish in a rigorous way for the system, (35), (36), applying to our billiard [a heuristic analysis yielding (34) is given in Sec. 7.2]. Thus, to make progress, we adopt a model system with the same structure as (35), (36). In particular, we wish to replace the two-dimensional billiard map (36) by a simpler map, $M_\phi \rightarrow \bar{M}_\phi$, that, like the original two-dimensional billiard map, is chaotic and describes a Hamiltonian system. For this purpose we choose the cat map,

$$\vec{\phi}_{n+1} = \bar{M}_\phi(\vec{\phi}_n) \equiv C\vec{\phi}_n \text{ modulo } 1, \quad (38)$$

where C is the cat map matrix,

$$C = \begin{bmatrix} 2 & 1 \\ 1 & 1 \end{bmatrix}.$$

Similarly, we replace $DM_z(0, \vec{\phi})$ in (35) by a simple symplectic map depending on $\vec{\phi}$,

$$\vec{z}_{n+1} = \bar{M}_z(\vec{z}_n) = \begin{bmatrix} \lambda & f(\vec{\phi}_n) \\ 0 & \lambda^{-1} \end{bmatrix} \vec{z}_n, \quad (39)$$

where $\lambda > 1$, and $f(\vec{\phi})$ is a smooth periodic function with period one in ϕ and π . [Note that vertical (i.e., parallel to z) line segments are uniformly expanded by the factor λ , and thus, by the same argument as in Sec. 3.1, we have $1/\tau = \ln \lambda$ and $h_z = 1/\tau$.]

Since only the angle of \vec{z} is needed to specify the stable manifold, we introduce the variable $\nu = z/v = \tan \chi$. We can then derive a map for ν : From (39) we have $\nu_{n+1}v_{n+1} = \lambda\nu_n v_n + v_n f(\vec{\phi}_n)$ and $v_{n+1} = \lambda^{-1}v_n$. Dividing the first equation by the second, v_{n+1} and v_n cancel and we obtain

$$\nu_{n+1} = \lambda^2 \nu_n + \lambda f(\vec{\phi}). \quad (40)$$

We now consider the dynamical system consisting of (38) and (40). Note that the system (38), (40) is a three-dimensional map, unlike the system (38), (39), which is a four-dimensional map.

For (38), (40), the stable manifold is given by

$$\nu = \nu_S(\vec{\phi}) = -\lambda^{-1} \sum_{i=0}^{\infty} \lambda^{-2i} f(C^i \vec{\phi}_0), \quad (41)$$

where C is the cat map matrix.

To verify that this is SM we note that points above SM , $\nu > \nu_S(\vec{\phi})$ [below SM , $\nu < \nu_S(\vec{\phi})$] are repelled toward $\nu \rightarrow \infty$ ($\nu \rightarrow -\infty$). Thus, on backwards iteration, points go toward SM . We take advantage of this behavior to determine SM . Imagine that we iterate $\vec{\phi}$ forward n iterates to $\vec{\phi}_n = C^n \vec{\phi}$ modulo 1, then choose a value of ν_n , and iterate it backwards using (40). We find that the initial value of ν at time zero giving the chosen value ν_n at time n is

$$\nu_0 = (\nu_n / \lambda^{2n}) - \lambda^{-1} \sum_{i=0}^{n-1} \lambda^{-2i} f(C^i \vec{\phi}).$$

Keeping ν_n fixed and letting $n \rightarrow +\infty$, the value of ν_0 approaches $\nu_S(\vec{\phi})$, given by (41).

Results proven in [10] show that the box-counting dimension (the capacity) of the graph of the function $\nu = \nu_S(\vec{\phi})$ given by (41) is

$$\hat{D}_S = \begin{cases} 3 - 2 \frac{\ln \lambda}{\ln B}, & \text{for } \lambda \leq B, \\ 2, & \text{for } \lambda > B, \end{cases} \quad (42)$$

where $B = \frac{3+\sqrt{5}}{2} > 1$ is the larger eigenvalue of the matrix C . The formula for $\lambda < B$ holds for almost all (with respect to Lebesgue measure) values of λ . Since $\lambda > 1$, the sum in (41) converges absolutely, implying that $\nu_S(\vec{\phi})$ is a continuous function of $\vec{\phi}$. Thus, when the first result in Eq. (42) applies (i.e., the surface is fractal with $\hat{D}_S > 2$), the stable manifold is a continuous nondifferentiable surface.

For example, evaluating (41) on the surface $\vec{\phi} = s \hat{u}_+$ where \hat{u}_+ is the unit vector in the eigendirection of C corresponding to the expanding eigenvalue B , we have that ν versus s is of the form

$$\nu = - \sum_{i=0}^{\infty} \lambda^{-2i} g(B^i s).$$

Thus, the graph of ν versus s for $B > \lambda$ has the form of Weierstraß's famous example of a continuous, nowhere-differentiable curve.

To obtain (42) in another way, we again consider the map (38), (40). We claim that (38), (40) can be regarded as a *typical* system, and that the formulae of Sec. 2 should apply to it. That is, in contrast to the existence of a symmetry for (39) [namely, $\vec{z} \rightarrow -\vec{z}$ leaves (39) invariant], (40) has no special symmetry.

The Lyapunov exponent corresponding to (40) is $h_\nu = 2 \ln \lambda$. Note that for the system (38), (40) [and also for the system (38), (39)] there are *no* fluctuations in the finite time Lyapunov exponents and thus the decay time for the system (38), (40) is given by $\tau_\nu^{-1} = h_\nu$. Noting that the Lyapunov exponents for the cat map are $\pm \ln B$ and applying (3) to the three-dimensional map (38), (40), we immediately recover Eq. (42). As discussed in Appendix B, this point of view can also be exploited for the original ellipsoid system [rather than just for the model system (38) and (39)].

Returning now to the full four-dimensional system, (38), (39), and noting that SM is smooth along the direction that we eliminated when we went from (38), (39) to (38), (40), we have that the dimension D_S of the stable manifold of the invariant set ($\vec{z} = 0$) for (38), (39) is $D_S = \hat{D}_S + 1$. The Lyapunov exponents for \vec{z} motion in the four-coordinate system are $\pm h_z = \pm \ln \lambda$ and $\pm h_\phi = \pm \ln B$ for $\vec{\phi}$ motion. In terms of the Lyapunov exponents, D_S is

$$D_S = \begin{cases} 4 - 2\frac{h_z}{h_\phi}, & \text{for } h_z/h_\phi \leq 1/2, \\ 3, & \text{for } h_z/h_\phi > 1/2. \end{cases} \quad (43)$$

Since $h_z = 1/\tau$ for (38) and (39) we see that, for $h_z/h_\phi \leq 1/2$, Eq. (43) is the same as Eq. (34). Also, the system (38), (39) has no finite time Lyapunov exponent fluctuations, and, thus, the information dimension and the box-counting dimensions are the same. Hence, $D_S = 3$ when SM is smooth ($h_z/h_\phi > 1/2$). This is analogous to the situation $r = 1$ and Eq. (24) of Sec. 3. [The lack of finite time Lyapunov exponent fluctuations for our model system (38), (39) is reflected in the fact that all periodic orbits in Λ have precisely the same Lyapunov exponents, namely $\pm \ln \lambda$ and $\pm \ln B$.]

6.2 Basin Boundary for a Map Modeling the Tilted Ellipsoid Billiard

We now wish to investigate the structure of the stable manifold when we give the ellipsoid a small tilt. Again, we adopt the approach of Sec. 4.2: we obtain a rigorous result by utilizing a simpler map model that preserves the basic features of the tilted ellipsoid case. Here we again use (38) but we now modify (39) to incorporate the main effect of a small tilt. The effect of this modification is to destroy the invariance of $\vec{z} = 0$. Thinking of the first non-zero term in a power series expansion for small $|\vec{z}|$, this invariance results because the first expansion term is linear in \vec{z} ; i.e., the \vec{z} -independent term in the expansion is exactly zero. When there is tilt this is not so. Thus we replace (39) by

$$\begin{bmatrix} z_{n+1} \\ v_{n+1} \end{bmatrix} = \begin{bmatrix} \lambda & f(\vec{\phi}_n) \\ 0 & \lambda^{-1} \end{bmatrix} \begin{bmatrix} z_n \\ v_n \end{bmatrix} + \begin{bmatrix} f_z(\vec{\phi}_n) \\ f_v(\vec{\phi}_n) \end{bmatrix}. \quad (44)$$

The simplest version of (44) which still has the essential breaking of $\vec{z} \rightarrow -\vec{z}$ symmetry is the case where $f = f_v = 0$. Because setting $f = f_v = 0$ greatly

simplifies the analysis, we consider this case in what follows (we do not expect our conclusion to change if $f, f_v \neq 0$). Thus, we have

$$\begin{bmatrix} z_{n+1} \\ v_{n+1} \end{bmatrix} = \begin{bmatrix} \lambda & 0 \\ 0 & \lambda^{-1} \end{bmatrix} \begin{bmatrix} z_n \\ v_n \end{bmatrix} + \begin{bmatrix} f_z(\vec{\phi}_n) \\ 0 \end{bmatrix}. \quad (45)$$

The problem of finding the stable manifold for the invariant set of the map, (38) and (45), is now the same as for the previously considered case of Eqs. (38) and (40) [compare the equation $z_{n+1} = \lambda z_n + f_z(\vec{\phi}_n)$ with (40)]. Thus, making use of this equivalence we can immediately write down the equation for the stable manifold in the four-dimensional state space (z, v, ϕ, ω) as

$$z = -v \sum_{i=0}^{\infty} \lambda^{-i} f_z(C^i \vec{\phi}), \quad (46)$$

which is obtained from (41) using the replacements $v \rightarrow z/v$, $\lambda f \rightarrow f_z$, and $\lambda^2 \rightarrow \lambda$. The rigorous results of Ref. [10] again show that this is a continuous, nowhere-differentiable surface for almost all λ in $1 < \lambda < B$, and, furthermore, when this is so ($\ln \lambda / \ln B = h_z/h_\phi \leq 1$) we have

$$D_S = 4 - \frac{h_z}{h_\phi}. \quad (47)$$

Also, $D_S = 3$ when $h_z/h_\phi > 1$. Since $h_z = 1/\tau$, this is the same as Eq. (33).

7 Derivation of Dimension Formulae

7.1 D_S for Typical Systems

While the dimension formulae presented in Sec. 2 and derived in [2] were found to be valid for the two-dimensional map of Sec. 3 and the ellipsoid scatterer of Secs. 4-6, the derivation given in [2] does not apply to these systems. In the derivation of [2], a higher-dimensional generalization of horseshoe-like dynamics is assumed. When this type of dynamics is responsible for a fractal basin boundary, the boundary looks, locally, like a Cantor set of smooth surfaces. The examples of this paper do not possess horseshoe-like dynamics. Their dynamics produces basin boundaries which consist of a single continuous surface; see Figs. 1, 5, and 7. We proceed to derive dimension formulae using a more general argument not restricted to an assumed particular type of boundary. The resulting formulae are identical to those derived in [2] and stated in Sec. 2.

Let R be the portion of the state space which contains all points within ϵ of a nonattracting, ergodic, invariant set, Λ of an M -dimensional map, P . Let sm be the portion of the stable manifold of Λ which is contained in R . The points in R are within ϵ of sm since Λ is a subset of sm . If we sprinkle a large number, N_0 , of orbit initial conditions in R , then the number of orbits left in R

after $n \gg 1$ iterates is assumed to scale like (3) $N_n/N_0 \sim e^{-n/\tau}$. Let the map, P , have Lyapunov exponents

$$h_U^+ \geq h_{U-1}^+ \geq \dots \geq h_1^+ > 0 > -h_1^- \geq \dots \geq -h_{S-1}^- \geq -h_S^-,$$

where $U + S = M$.

We will use the box-counting definition of dimension

$$N(\epsilon) \sim \epsilon^{-D}, \quad (48)$$

where $N(\epsilon)$ is the minimum number of M -dimensional hypercubes (“boxes”) needed to cover sm and D is its box-counting dimension.

We wish to develop a covering of sm using small boxes and determine how the number of boxes in that covering scales as the size of the boxes is decreased. We will look at how the linearized system dynamics distorts a typical small box. This will help us determine how the Lyapunov exponents are related to the dimension of sm . Since we assume a smooth map, the dimension of the stable manifold of the map is equal to that of sm .

Cover sm with boxes which are of length ϵ on each of their M sides. Call this set of boxes C . The number of boxes in C is denoted N_0 . Iterate each box forward n steps, where n is large, but not so large that the linearized dynamics do not apply to the boxes. Call the set of iterated boxes $P^n(C)$. A typical iterated box in $P^n(C)$ is a distorted M -dimensional parallelepiped and has dimensions

$$\epsilon e^{nh_U^+} \times \dots \times \epsilon e^{nh_1^+} \times \epsilon e^{-nh_1^-} \times \dots \times \epsilon e^{-nh_S^-}.$$

Each parallelepiped intersects sm since its preimage (a box) did. (The set $P^n(C)$ does not, however, cover all of sm since points on sm move closer to Λ on forward iteration.)

To construct a refined covering of sm we begin by covering each parallelepiped of $P^n(C)$ with slabs of size

$$\frac{U \text{ factors}}{\epsilon \times \dots \times \epsilon} \times \epsilon e^{-nh_1^-} \times \dots \times \epsilon e^{-nh_S^-}.$$

There are roughly $\exp[n(h_U^+ + \dots + h_1^+)]$ such slabs. Only $\sim e^{-n/\tau}$ of these slab are within ϵ of sm . Let C' denote the set of $N' \sim N_0 \exp[n(h_U^+ + \dots + h_1^+ - 1/\tau)]$ slabs needed to cover the part of sm lying in $P^n(C)$. Let us define $H = h_U^+ + \dots + h_1^+ - 1/\tau$ so that $N' \sim N_0 e^{nH}$.

Iterate each of the N' slabs backward n steps. We now have the set $P^{-n}(C')$. It contains N' parallelepipeds of size

$$\epsilon e^{-nh_U^+} \times \dots \times \epsilon e^{-nh_1^+} \times \frac{S \text{ factors}}{\epsilon \times \dots \times \epsilon}.$$

The set $P^{-n}(C')$ forms a covering of sm . To calculate the dimension (which is defined in terms of boxes) we cover the N' parallelepipeds in $P^{-n}(C')$ with

boxes which are $\epsilon_j = \epsilon e^{-nh_{j+1}^+}$ on each side. (We will choose the value of the index j below.) The number of boxes needed to cover sm , for boxes of size ϵ_j , scales as

$$N'' \sim N' \frac{\epsilon e^{-nh_j^+}}{\epsilon_j} \times \frac{\epsilon e^{-nh_{j-1}^+}}{\epsilon_j} \times \cdots \times \frac{\epsilon e^{-nh_1^+}}{\epsilon_j} \times \left(\frac{1}{\epsilon_j}\right)^S.$$

To cover the slabs with these boxes we need a factor of 1 boxes along each direction of a slab which is shorter than the edge length of a box and a factor of $\epsilon e^{-nh_k^+}/\epsilon_j$ boxes along each direction (here, the k^{th} direction) which is longer than the edge length of a box. In terms of N_0 ,

$$N'' \sim N_0 \exp\{n[(S+j)h_{j+1} + H - h_1^+ - h_2^+ \cdots - h_j^+ - 1/\tau]\}.$$

To compute the dimension of sm , we compare $N(\epsilon) \equiv N_0$ to $N(\epsilon_j) \equiv N''$ using (48). This gives $N(\epsilon_j)/N(\epsilon) \sim (\epsilon/\epsilon_j)^D \sim \exp(nDh_{j+1}^+)$ which yields the following j -dependent dimension estimate,

$$D(j) = S + j + \frac{H - h_1^+ + h_2^+ + \cdots + h_j^+}{h_{j+1}^+}. \quad (49)$$

Our definition of box-counting dimension, (48), requires us to find the minimum number of boxes needed to cover the set. Since we are certain that the set is covered, (49) yields an upper bound for the dimension for any j . Thus, to find the best estimate of those given by (49), we minimize $D(j)$ over the index j . Comparing $D(j)$ to $D(j+1)$ yields the condition

$$h_1^+ + \cdots + h_j^+ + h_j^+ \geq H \geq h_1^+ + \cdots + h_j^+,$$

where J is the best choice for j (i.e., the choice giving the minimum upper bound). The conjecture is that this minimum upper bound $D(J)$ from (49) is the actual dimension of sm for typical systems. $D(J)$ is the same as the result Eq. (8) presented in Sec. 2 for D_S . The derivation of the dimension formula for the unstable manifold, D_U , is similar to that just presented for the stable manifold.

[The derivation just presented gives the *information* dimension of the stable manifold, not the box-counting dimension. We were considering the sizes of typical boxes in the system and covered only those. This leaves boxes that have atypical stretching rates for large n (a box containing a periodic point, for example, will, in general, not stretch at the rates given by the Lyapunov exponents) unaccounted for. What we have actually computed is the box-counting dimension of most of the measure, which is the information dimension [11], of the stable manifold. See [11] for discussion of this point.]

As derived, $D(J)$ gives an upper bound on the dimension. We saw in the ellipsoid example of Secs. 4-6 that the $z \rightarrow -z$ symmetry of the system lead to a special geometry for its stable manifold (Fig. 7) and the formula just derived did not apply (although it was an upper bound). It is the conjecture of [2] that this formula gives not the upper bound, but the exact dimension of the stable manifold for typical systems. This is supported by our results for the tilted ellipsoid example.

7.2 D_S for the Untilted (Atypical) Case

The derivation above for typical systems gives the wrong dimension formula for the stable manifold of the (atypical) untilted ellipsoid system. This typical-system derivation consistently overcounts the boxes needed to cover the atypical stable manifold of the untilted ellipsoid system. Sec. 6.1 showed that the stable manifold had a ray-like structure (cf. Fig. 7) induced by the z -direction reflection symmetry of the system. If we account for this structure we can modify the typical-system derivation so that we do not overcount boxes. The modified derivation produces the correct formula.

Recall that our untilted ellipsoid map (which we call P here) has Lyapunov exponents $\pm h_z$ and $\pm h_\phi$ and decay time τ . We consider the case

$$h_\phi > h_z + \tau > 0$$

Let us cover the region of state space which is within $\epsilon/2$ of Λ with N_0 boxes with edge lengths $\epsilon \times \epsilon \times \epsilon \times \epsilon$. Call this set C . The map, P , is linear in \vec{z} (in particular, the \vec{z} portion is of the form $\vec{z}_{n+1} = DM(\vec{\phi})\vec{z}_n$) so that the graph of SM in \vec{z} space for a given value of $\vec{\phi}$ is a straight line through $\vec{z} = 0$, i.e. $z = vg(\vec{\phi})$. We denote by sm the portion of the stable manifold which is contained in C . Since SM contains Λ , each box in C intersects sm .

Iterate these boxes forward $n \gg 1$ steps. They become a set distorted of parallelopipeds which we call $P^n(C)$. Each parallelopiped has dimensions

$$\epsilon e^{nh_\phi} \times \epsilon e^{nh_z} \times \epsilon e^{-nh_z} \times \epsilon e^{-nh_\phi}$$

and intersects sm . We cover $P^n(C)$ by $N_0 \exp[n(h_z + h_\phi)]$ parallelopipeds with dimensions

$$\epsilon \times \epsilon \times \epsilon e^{-nh_z} \times \epsilon e^{-nh_\phi},$$

and discard all of these parallelopipeds which do not intersect sm . There are $N' \sim N_0 \exp[n(h_z + h_\phi - 1/\tau)]$ parallelopipeds remaining which cover sm . The portions of these parallelopipeds which are in $\epsilon > |z| > \epsilon e^{-nh_z}$ do not contain sm . Suppose some portion of sm did fall in $\epsilon > |z| > \epsilon e^{-nh_z}$. Since P is linear in \vec{z} , this outlying portion of sm would, upon n reverse iterations, map to the region $\epsilon e^{nh_z} > |z| > \epsilon$, which contradicts the definition of sm given above (i.e. sm is within $\epsilon/2$ of Λ). Therefore we can discard the portion of each parallelopiped which lies in $\epsilon > |z| > \epsilon e^{-nh_z}$. These N' parallelopipeds now have dimensions

$$\epsilon \times \epsilon e^{-nh_z} \times \epsilon e^{-nh_z} \times \epsilon e^{-nh_\phi},$$

and are denoted C' . We now iterate the parallelopipeds in C' backward n times and call the resulting set $P^{-n}(C')$. This set contains N' parallelopipeds with dimensions

$$\epsilon e^{-nh_\phi} \times \epsilon e^{-2nh_z} \times \epsilon \times \epsilon.$$

We cover $P^{-n}(C')$ (which covers sm) with hypercubes which have as their edge length ϵe^{-nh_ϕ} . The number of hypercubes needed is $N'' \sim N_0 \exp[n(h_z + h_\phi -$

$1/\tau - 2h_z + 3h_\phi$]. The (information) dimension is again found by comparing the number of ϵ -sized hypercubes needed to cover sm to the number of ϵe^{-nh_ϕ} sized hypercubes needed to cover sm ,

$$\frac{N''}{N_0} \sim \left(\frac{\epsilon e^{-nh_z}}{\epsilon} \right)^{-D},$$

which yields

$$D = 4 - \frac{h_z + 1/\tau}{h_\phi}.$$

This expression is between three and four for $(h_z + 1/\tau)/h_\phi < 1$.

8 Discussions and Conclusions

In summary, this paper has tested and illustrated formulae giving the fractal dimension of nonattracting chaotic sets in terms of their Lyapunov exponents and decay time. We have done this using two examples, one, a noninvertible, two-dimensional map with two expanding (positive) Lyapunov exponents, and the other, a chaotic scattering billiard in three spatial dimensions. The first example is particularly useful for understanding the transient measure. The second example provides a striking illustration of the issue of atypicality, and also has the benefit of potential physical realization (see below). Another point is that our second example provides the first known case of a chaotic scatterer with a fractal basin boundary that is a continuous, nowhere-differentiable surface (such structures have been previously discussed for basins of attraction of dissipative systems but not in chaotic scattering). Finally, in Sec. 7 we have provided arguments that are more general than those previously given [2] for the dimension formulae of Sec. 2.

To conclude, we now offer some discussion on the possible experimental realization of our billiard example. Our point here is that such billiard systems offer a particularly nice way of experimentally realizing and studying basin boundaries. In the past there have been very few experiments that have attempted to study basin boundaries. The problem is the experimental difficulty of carrying out the technique used in numerical work: namely, choosing a grid of initial conditions and seeing where each orbit from each initial condition goes. To do this experimentally, one would have to precisely prepare an initial condition, run the experiment to see where the orbit with that initial condition goes, and do this for each initial condition. The difficulties with this approach are that it is often not possible to prepare initial conditions either on a fine enough grid or sufficiently precisely to observe small scale basin boundary structures and that running the experiment many times can be time consuming. (In addition, experimental parameters may drift over the course of the multiple experimental runs.) Nevertheless, in one case [13] this program was successfully carried out. In that paper an electrical circuit was used as the experimental chaotic system, and the authors were able to experimentally demonstrate a riddled basin of attraction

(a type of basin for which final outcomes are particularly difficult to predict; see Refs. [14], [15]). In another work, Cusumano and Kimble [16] have devised a new experimental procedure for studying basin boundaries. This procedure has advantages over the straightforward method of preparing initial conditions on a grid. Using this method, Cusumano and Kimble have successfully mapped out basin boundaries for experimental dissipative mechanical systems. To our knowledge, these two works (and a billiard we discuss below) are so far the only experimental investigations of fractal basin boundaries. This is in contrast to the large number of papers that have experimentally realized fractal structure in chaotic attractors. This disparity in the situations of attracting and nonattracting chaotic sets seems to be largely due to the disparity in the ease of experimental realization for the two cases.

We believe that billiard systems offer a convenient avenue for experimental investigation of the various general types of basin boundaries. In particular, we suggest an optical realization of chaotic scattering billiards in which the billiard surface is made to be optically reflecting, and light rays play the role of orbits. For the scatterer of Sec. 4-6, for example, imagine that we have a tube with cross section as shown in Fig. 4(b) and mirrored inner walls. The length of the tube is $L > 2r_{\perp}$, where r_{\perp} is the major radius of an ellipsoid with a mirrored surface. Imagine that the tube is oriented vertically with its bottom, open end placed on a red surface, and that the ellipsoid is suspended in the tube. In this configuration, an observer looking in the top of the tube sees multiple reflections of the red surface that is at the bottom of the tube. Since rays whose directions are reversed retrace the same path, we can think of orbits from initial conditions starting on the retina of the observer's eye passing through his pupil, bouncing around in the scatterer, and then exiting either through the bottom (red) or the top (not red). Thus, the observed boundary of the red region is precisely the basin boundary that we have been discussing in Secs. 4-6. Note that to observe that boundary we did not have to prepare many initial conditions and repeat the experiment many times. Rather a single image giving a global picture of the basin can be formed (replacing the observer's eye by a camera). We have already applied this approach to a chaotic scatterer formed from four mirrored spheres to experimentally study a different general type of basin boundary structure known as a Wada boundary [17] (a Wada boundary is a boundary separating three or more regions such that every boundary point is a boundary point for all regions). In the case of our ellipsoid billiard, such an experiment would represent the first experimental realization of a fractal basin boundary with the structure of a continuous, nowhere-differentiable surface, one of the small number of typical possible basin boundary types [1].

We thank J. A. Yorke and B.R. Hunt for discussion. This work was supported by ONR and DOE.

Appendix A: Slow Convergence of the Dimension Near the Transition Between Fractal and Non-fractal Behavior

It is difficult to numerically measure the box-counting dimension of the chaotic repellers studied in Sec. 3 and Secs. 4-6 for some range of the system parameter. When the parameter is set near the value at which the repellor makes the transition from a fractal to a non-fractal function the number of boxes needed to cover the set scales as

$$N(\epsilon) \sim \frac{[\ln(1/\epsilon)]^{\frac{1}{2}}}{\epsilon^{D_0}} \quad (\text{A1})$$

with ϵ (the width of a box) down to very small ϵ . In (A1), $D_0 = 1$ in the case of the two-dimensional map and $D_0 = 3$ in the case of the ellipsoid system. Due to the logarithmic term in (A1) accurate numerical determination of D_0 can be very demanding. In the following we demonstrate that (A1) holds near the transition point between a fractal and a nonfractal. In particular, we consider (13)-(15) [$D_0 = 1$ in Eq. (A1)] in the case where $\lambda_1 = \lambda_2 = \lambda$. Using the same reasoning as for the derivation of Eq. (41) we obtain for the invariant set the curve

$$y(x) = -\frac{\eta}{2\pi} \sum_{i=0}^{\infty} \lambda_i^{-1} \sin(2\pi 2^i x). \quad (\text{A2})$$

This result is also derived in Ref. [1]. The box-counting dimension of the graph of $y(x)$ versus x is [1] $D_0 = 2 - [\ln \lambda / \ln 2]$ for $\lambda \leq 2$ and $D_0 = 1$ for $\lambda \geq 2$. Thus, the graph of $y(x)$ is a fractal for $\lambda \leq 2$ and is non-fractal for $\lambda \geq 2$. We are interested in the transition region, $\lambda \cong 2$, for which we wish to show that (A1) applies.

To calculate the box-counting dimension of (A2) we need to know how the number of ϵ -width boxes needed to cover the set scales with ϵ . If we let the sum in (A2) run from $i = 0$ to $i = n$, the resulting approximation to $y(x)$ is a smooth, finite length curve:

$$y_n(x) = -\frac{\eta}{2\pi} \sum_{i=0}^n \lambda^{-i} \sin(2\pi 2^i x). \quad (\text{A3})$$

As n increases, the ratio of the height to the width of the oscillations added by each term in the sum increases. For the purpose of estimating $N(\epsilon)$ for some fixed value of ϵ it suffices to consider (A3) with n sufficiently large. A practical size for the boxes in a covering is one which scales as the width of the smallest oscillations of (A2): $\epsilon_n \sim 2^{-n}$. This way we can be sure to resolve the smallest details of the approximation curve (A3) and be sure that higher order approximations will not significantly alter our count of the number of boxes in the covering. (Oscillations introduced by the $n + 1^{\text{st}}$ term, for example, will be roughly half the width of a box of size $\epsilon_n \sim 2^{-n}$, or $\sim 2^{-(n+1)}$.)

The length of the curve (A3) is

$$\ell_n = \int_0^1 dx \sqrt{1 + [y'_n(x)]^2} \equiv \left\langle \sqrt{1 + [y'_n(x)]^2} \right\rangle,$$

where $\langle \bullet \rangle$ denotes an average over x . For large n and $\lambda \leq 2$, $|y'_n(x)|$ is typically large and $\ell_n \cong \langle |y'_n(x)| \rangle$.

To determine ℓ_n we examine

$$y'_n(x) = -\eta \sum_{i=0}^n \left(\frac{2}{\lambda} \right)^i \cos(2\pi 2^i x).$$

For $\frac{2}{\lambda}$ sufficiently large, the largest term in this sum dominates and $y'_n(x) \approx \left(\frac{2}{\lambda}\right)^n$. In this case, $\ell_n \sim \left(\frac{2}{\lambda}\right)^n$ and $N(\epsilon_n) \sim \frac{\ell_n}{\epsilon_n}$. Taking $\epsilon = 2^{-n}$, or $n = -\ln \epsilon / \ln 2$ we have that $N(\epsilon) \sim \epsilon^{-(2 - \ln \lambda / \ln 2)}$. The scaling is a power law in ϵ . (It gives a box-counting dimension of $D_0 = 2 - \ln \lambda / \ln 2$.)

For $\lambda < 2$, but $\lambda \approx 2$, the last term will not dominate the sum, but the last several, up to n_x , terms will dominate. To estimate n_x , set $\left(\frac{2}{\lambda}\right)^{n_x}$ equal to a constant factor $K > 1$ where $K - 1$ is order one (e.g., $K = 2$). This gives $n_x \sim (2 - \lambda)^{-1} \gg 1$. If $n \leq n_x$, then all the coefficients $(2/\lambda)^i$ in the sum $y'_n(x)$ are of the same order, $y'_n(x) \sim \sum_{i=0}^n \cos(2\pi 2^i x)$. For a given value of x and different values of $i \gg 1$ the arguments of the cosine terms in the sum are very different and vary rapidly with x . Thus, we regard the terms in the sum as random. In this case $y'_n \sim \sqrt{n}$, and, thus, $\ell_n \sim \sqrt{n}$. Again, we say that $N(\epsilon_n) \sim \frac{\ell_n}{\epsilon_n}$, but now $N(\epsilon_n) \sim \sqrt{n}/\epsilon_n \sim \sqrt{-\ln \epsilon_n / \epsilon_n}$, which is (A1). If $n > n_x$, then $|y'_n(x)| \sim n_x^{1/2} \left(\frac{2}{\lambda}\right)^n$.

For the two-dimensional example studied numerically in Sec. 3.3, the numerical results are shown in Fig. 2. Due to the effect discussed in this appendix we have not plotted data near the kink at $\lambda_1 = \lambda_b$. The results for the ellipsoid system are discussed in Sec. 5 and shown in Fig. 6. A typical two-dimensional slice of the basin boundary for this system is a continuous, nowhere-differentiable curve similar to the chaotic saddle of the two-dimensional system. We thus have the same difficulty in measuring the dimension near $h_\phi \tau = 1$, Fig. 6(a) and $h_\phi = h_z + \tau^{-1}$ Fig. 6(b).

Appendix B: Dynamics of the Orientation of \vec{z}

Rewriting (35) as,

$$z_{n+1} = m_{11}(\vec{\phi}_n)z_n + m_{12}(\vec{\phi}_n)v \quad (\text{B1})$$

$$v_{n+1} = m_{21}(\vec{\phi}_n)z_n + m_{22}(\vec{\phi}_n)v_n, \quad (\text{B2})$$

eliminating z in favor of $v = z/v$, and dividing the first of the above equations by the second, v_{n+1} and v_n cancel to yield an evolution equation for v ,

$$v_{n+1} = \frac{m_{11}(\vec{\phi}_n)v_n + m_{12}(\vec{\phi}_n)}{m_{21}(\vec{\phi}_n)v_n + m_{22}(\vec{\phi}_n)}. \quad (\text{B3})$$

Equations (36) and (B3) now constitute a 3D map. Our transformation from (B1), (B2) eliminates the symmetry of the original system, and it is reasonable to now assume that the information dimension of the natural transient measure for the 3D map (36) and (B3) is given by the result for a typical system. Thus, we have that the information dimension of the stable manifold of the invariant set for the 3D map is

$$\hat{D}_S = 3 - (\hat{h}_\phi \hat{\tau})^{-1}, \text{ for } \hat{h}_\phi \hat{\tau} \geq 1. \quad (\text{B4})$$

Where the superscribed circumflex denotes quantities calculated for the natural transient measure of the 3D map, (36) and (B3). Since the information dimension \hat{D}_S is a lower bound on the box-counting dimension for the map (36) and (B3), and since the box-counting dimension of SM for the original 4D map is one plus that for the 3D map (this follows from the structure shown in Fig. 7), we have that $\hat{D}_S + 1$ [with \hat{D}_S given by (B4)] is a lower bound for the box-counting dimension of SM for the 4D map. We emphasize, however, that $\hat{D}_S + 1$ is different from D_S for the 4D system. This is because of the difference in the natural transient measures for the 3D and 4D maps. (In contrast, the box-counting dimensions do not depend on the measures.) In particular, as shown below, as compared to the 4D map natural transient measure, the natural transient measure for the 3D map more strongly weights $\vec{\phi}$ values which experience slower repulsion from the invariant set Λ .

To see this we consider the Lyapunov exponent corresponding to the evolution of a differential perturbation in ν which we denote $\delta\nu$. Differentiating (B3) we have

$$\delta\nu_{n+1}/\delta\nu_n = \bar{d}(\vec{\phi}_n)(m_{21}\nu_n + m_{22})^{-2}, \quad (\text{B5})$$

where $\bar{d}(\vec{\phi}_n)$ the determinant of (B1), (B2), $\bar{d}(\vec{\phi}_n) = m_{11}m_{22} - m_{12}m_{21} = 1$. Noting that $\nu_n = z_n/\nu_n$ and comparing (B5) with (B2), we have

$$\delta\nu_{n+1}/\delta\nu = \bar{d}(\vec{\phi}_n)(v_n/v_{n+1})^2. \quad (\text{B6})$$

For points on SM , v_n decreases exponentially with time (i.e., it approaches the invariant set Λ). Hence,

$$\delta\nu_n/\delta\nu_0 = Q(v_n/v_0)^{-2} \sim \exp[2n\tilde{h}_z(\vec{\phi}_0, n)], \quad (\text{B7})$$

where $Q = \bar{d}(\vec{\phi}_0)\bar{d}(\vec{\phi}_1)\dots\bar{d}(\vec{\phi}_{n-1})$ and $\tilde{h}_z(\vec{\phi}, n)$ with $\vec{\phi} = \vec{\phi}_0$ is the expanding \vec{z} , finite-time Lyapunov exponent for the 4D system. The estimate, $\exp(2n\tilde{h}_z)$, in (B7) follows since, due to the Hamiltonian nature of the problem, $Q^{1/n} \rightarrow 1$ as $n \rightarrow \infty$. Thus, for a given value of $\vec{\phi}$, in the 3D system, the expansion away from the invariant set is at the rate $2\tilde{h}_z(\vec{\phi}, n)$ rather than at the rate $\tilde{h}_z(\vec{\phi}, n)$, applying to the 4D system. For the example of (39) there are no finite time Lyapunov exponent fluctuations [$\tilde{h}_z(\vec{\phi}, n) = \ln \lambda$ independent of n and $\vec{\phi}$], so that the 3D and 4D natural transient measures are the same, both are uniform in $\vec{\phi}$.

In this case,

$$\hat{\tau} = \tau/2 = (\ln \lambda)^{-1}. \quad (\text{B8})$$

More generally, the finite time exponents, $\tilde{h}_z(\vec{\phi}, n)$, fluctuate as $\vec{\phi}$ varies. The faster expansion rate away from Λ (namely $2\tilde{h}_z$) in the 3D case means that $\vec{\phi}$ values with slower expansion rates are more strongly weighted. Thus, for a case such as our ellipsoid problem we expect that

$$\hat{\tau} > \tau/2 \hat{h}_\nu < 2h_z,$$

where \hat{h}_ν is the infinite time Lyapunov exponent for the 3D map measure and for perturbations in ν .

References

- [1] S. W. McDonald, C. Grebogi, E. Ott, and J. A. Yorke, *Physica D* **17**, 125 (1985).
- [2] B. R. Hunt, E. Ott, J. A. Yorke, *Phys. Rev. E* **54**, 4819 (1996).
- [3] H. Kantz and P. Grassberger, *Physica D* **17**, 75 (1985).
- [4] G. H. Hsu, E. Ott, and C. Grebogi, *Phys. Lett. A* **127**, 199 (1988).
- [5] M. Ding and E. Ott, *Ann N.Y. Acad. Sci.* **751**, 182 (1995).
- [6] J. L. Kaplan and J. A. Yorke, in *Functional Differential Equations and Approximations of Fixed Points*, edited by H.O. Peitgen and H.O. Walter, *Lecture Notes in Mathematics Vol. 730* (Springer, Berlin, 1979), p. 204.
- [7] L.-S. Young, *Ann. Math.* **122**, 509 (1985); **122**, 540 (1985).
- [8] F. Ledrappier, *Commun. Math. Phys.* **81**, 229 (1981).
- [9] P. Frederickson, J. L. Kaplan, E. D. Yorke, J. A. Yorke, *J. Diff. Eq.* **49**, 185 (1983).
- [10] J. L. Kaplan, J. Mallet-Paret, and J. A. Yorke, *Ergod. Th. Dynam. Sys.* **4**, 261 (1984).
- [11] E. Ott, *Chaos in Dynamical Systems* (Cambridge University Press, Cambridge, 1993).
- [12] S. Pelikan, *Trans. Amer. Math. Soc.* **292**, 695 (1985).
- [13] J. F. Heagy, T. L. Carroll, and L. M. Pecora, *Phys. Rev. Lett.* **72**, 3528 (1994).
- [14] J. C. Alexander, J. A. Yorke, Z. You, I. Kan, *Int. J. Bifurcations and Chaos* **2**, 795 (1992).
- [15] E. Ott, J. C. Alexander, I. Kan, J. C. Sommerer, and J. A. Yorke, *Physica (Amsterdam)* **76D**, 384 (1994).

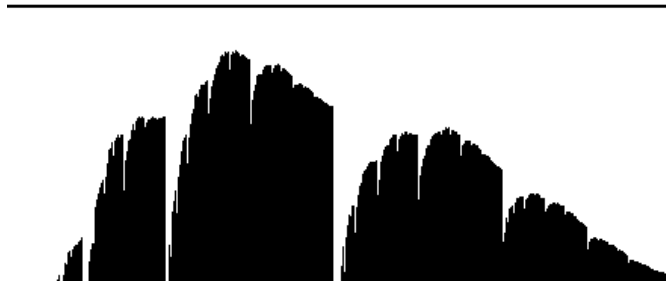


Figure 1: Basins of 2D map model, Eqs. (13)-(15) for $\lambda_1 = 1.1$, $r = 3$. A 500x500 grid of initial conditions was chosen in $0 \leq x \leq 1$, $-0.3 \leq y \leq .2$. Each was iterated forward by the 2D map until the orbit fell in one of the regions $|y| > 5$. If the orbit fell in $y > 5$ ($y < -5$) a white (black) point was plotted on the initial condition grid shown above. The dimension of the boundary between black and white (the basin boundary) is $D \approx 1.28$.

- [16] J. P. Cusumano and B. W. Kimble, *Nonlin. Dyn.* **8**, 213 (1995).
- [17] D. Sweet, E. Ott, J. A. Yorke, *Nature* **399**, 315 (1999).
- [18] H. D. I. Abarbanel, *Analysis of Observed Chaotic Data* (Springer, New York, 1996). For orbits lasting fewer than 25 iterates we use the “recursive QR decomposition” method described in section 5.6.1.

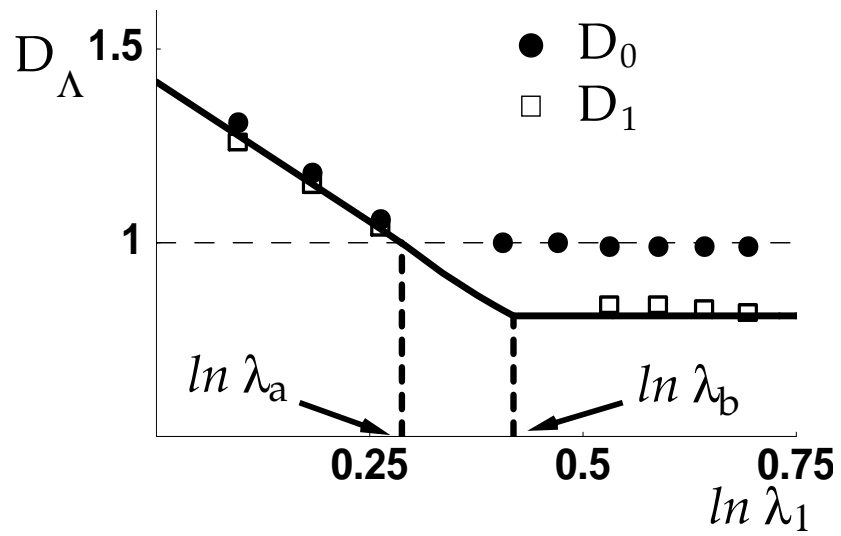


Figure 2: Comparison of prediction and numerical dimension calculations for the 2D model map, (13)-(15), with $r = \lambda_2/\lambda_1 = 3$ fixed. The filled dots show calculations of the box-counting dimension, and the boxes show information dimension. The solid line shows the predicted information dimension as given by Eqs. (21)-(23).

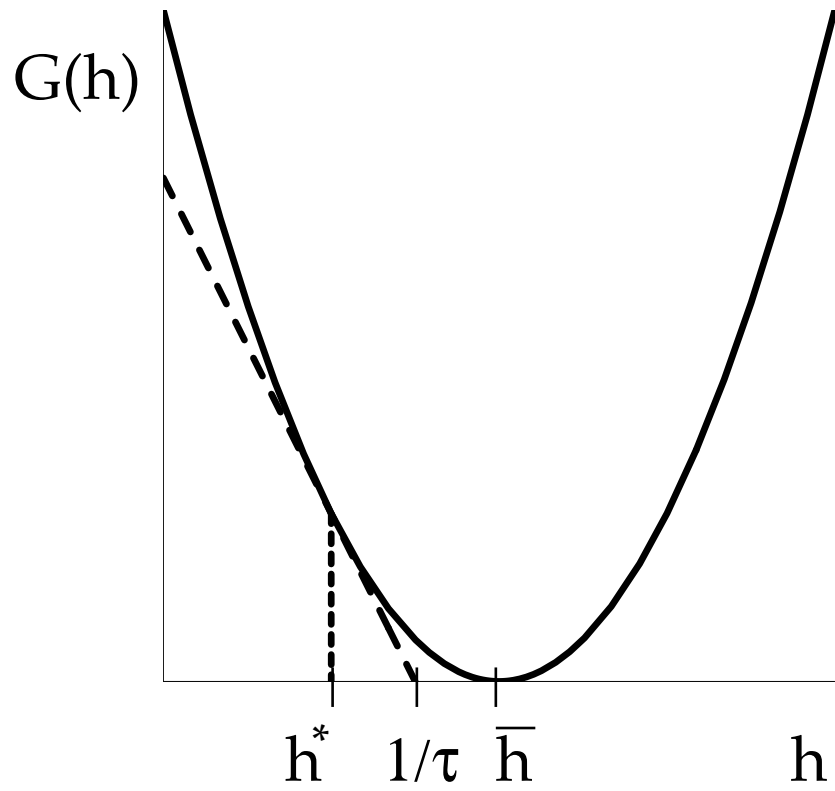


Figure 3: $G(h)$ versus h . The long-dashed line has slope -1 and is tangent to the graph of $G(h)$ at the point $h = h_*$.

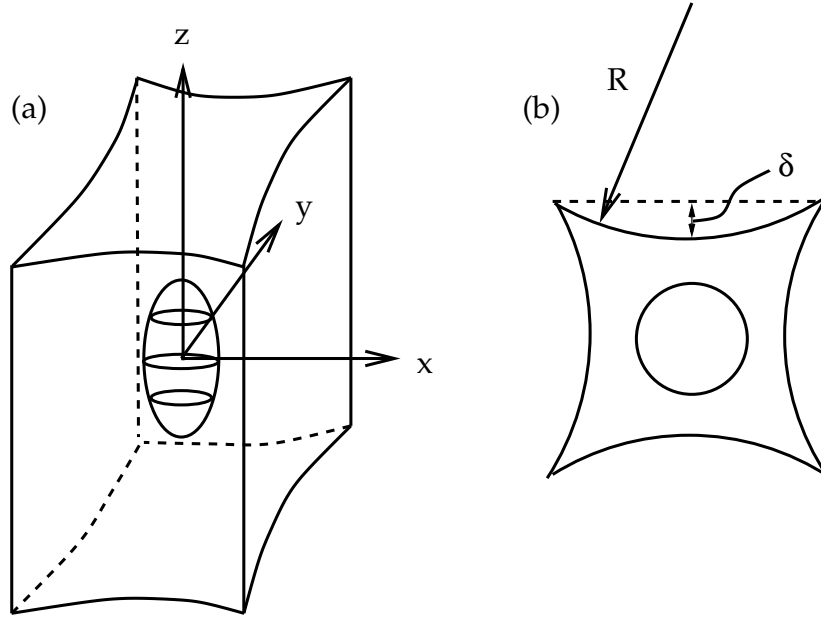


Figure 4: The scattering system in the (atypical) case of vertical orientation of the ellipsoid. (a) A hard ellipsoid is placed inside a hard tube with cross-section as shown in (b). (The circle in (b) is the cross section of the ellipsoid.) $R = 25$, $d = 10$ and the radius of the ellipsoid at $z = 0$ is $r_{\parallel} = 5$.

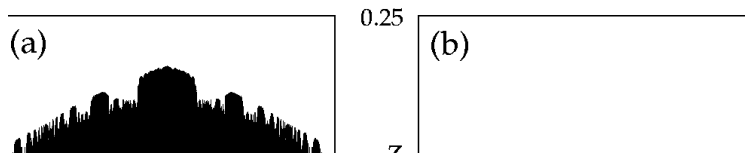


Figure 5: Basins for $z \rightarrow \infty$ (white) and $z \rightarrow -\infty$ (black). $r_{\perp} = 7$, $y = 5.1$, $4v_x = 0$, $v_z = .1$, and v_y is given by the condition $|\vec{v}| = 1$ for (a) the untitled case and (b) a tilt of $\frac{2\pi}{100}$.

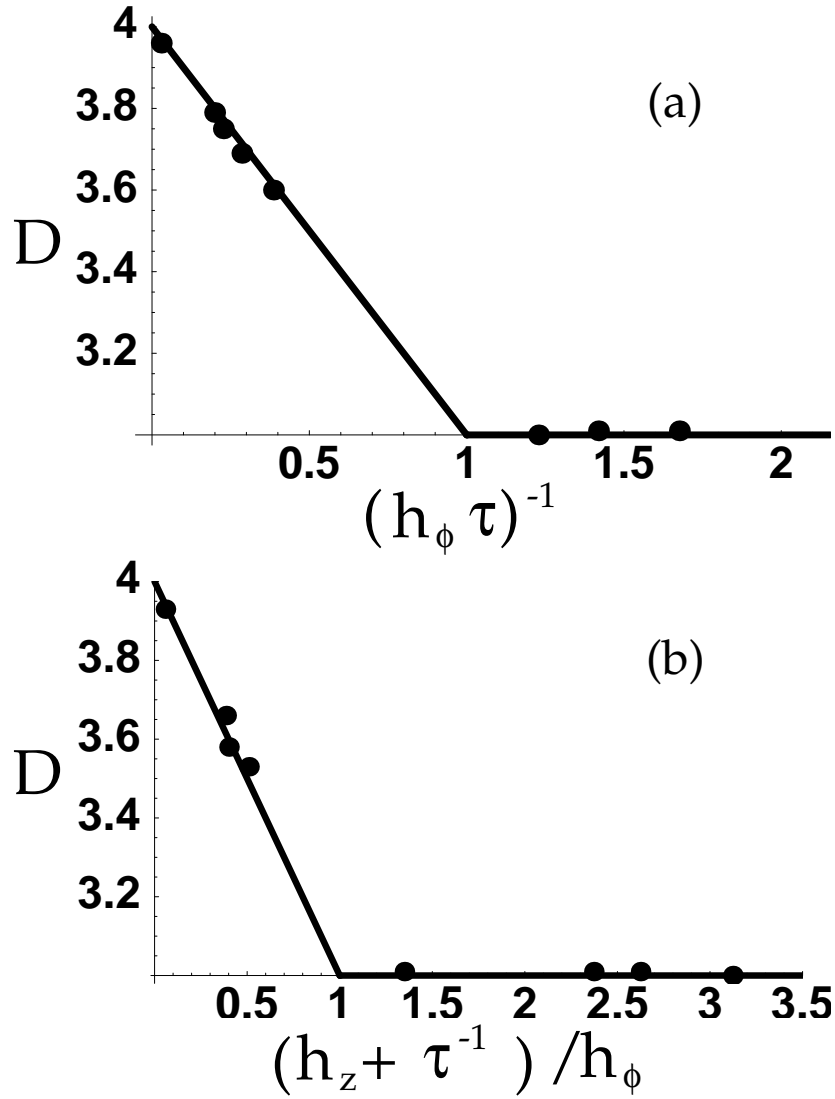


Figure 6: Comparison of dimension formulae, Eq. (33) and (34), with numerical estimates. The lines are the graphs of the equations and the dots show the numerical estimates of the box-counting dimension. (a) The tilted ellipsoid (typical) case. (b) The untilted ellipsoid (atypical) case.

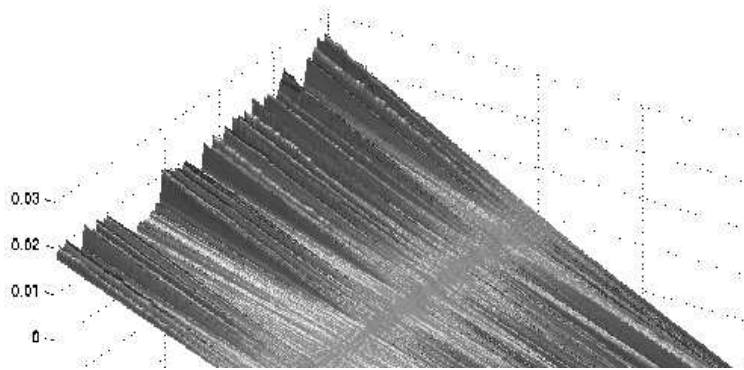


Figure 7: Stable manifold (SM) of the chaotic saddle (Λ); $r_{\perp} = 15$, $y = 5.1$, $v_x = 0$, and v_y is given by the condition $|\vec{v}| = 1$. The $v_z = 0$, $z = 0$ line is Λ . Notice the organization of SM into rays emanating from Λ . This special structure is atypical and is used to derive the atypical dimension formula for SM , Eq. (34).

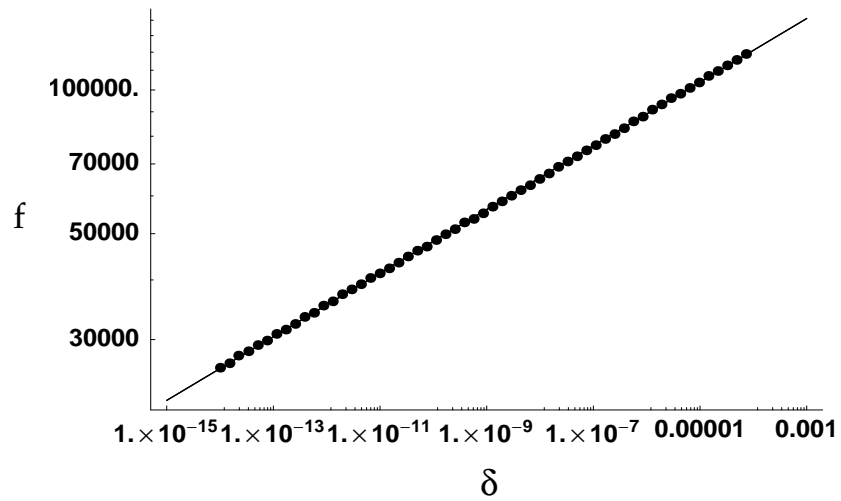


Figure 8: Uncertainty dimension measurement for the untilted ellipsoid system with $r_{\perp} = 100$. Plotted is the fraction of a random sample of points which are “ $|\vec{\delta}|$ -uncertain” for various values of $|\vec{\delta}|$. The line running through the dots is a linear fit with a slope of $\approx .07$, yielding a dimension of $d_0 \approx 2 - .07 = 1.93$.